Carbide Derived Carbon Coatings

on Carburized Ti-6Al-4V Surfaces by Molten Salt Electrolysis

BY

LEQING YANG

THESIS

Submitted as partial fulfillment of the requirements

for the degree of Master of Science in Materials Engineering

in the Graduate College of the

University of Illinois at Chicago, 2019

Chicago, Illinois

Defense Committee:

Michael McNallan, UIC Civil and Materials Engineering, Chair and Advisor

Eduard Karpov, UIC Civil and Materials Engineering, Associate Professor

Matthew Daly, UIC Civil and Materials Engineering, Assistant Professor

ABSTRACT

Carbide Derived Carbon (CDC) is a porous nano-material that have been used in gas storage, battery, and supercapacitor. Chlorine gas is used to produced CDC on the substrate by etching it. However, chlorine is toxic and not environmentally friendly, and also difficult to transport. Also, the temperature and time in this process is hard to use in industry. This study is focus on an environmental friendly and effective method using reactive anode electrolysis in molten chloride salts is presented as an alternative process for synthesizing CDC. The results shown by Raman spectroscopy shows that this method can produce CDC coatings on TI-6Al-4V substrate.

ACKNOWLEDGMENTS

I would like to thank my supervisor Michael McNallan for his comments, assistance and engagement during the time of this master thesis. Also, I would like to thank Kai-yuan Cheng and Yani Sun, help me to learn the topic and for the support during the whole process. Also, I would like to thank my parents, who have supported me during the whole process.

Table of Content

List of Tables

List of Figures

LIST OF ABBREVIATIONS

a-C Amorphous Carbon

AES Auger Electron Spectroscopy

CDC Carbide Derived Carbon

CNT Carbon Nanotube

CVD Chemical Vapor Determination

GFE Gibbs Free Energy

JANAF Joint Army Navy Air Force

NCG Nanocrystalline Graphite

NIST National Institute of Standards and Technology

SC Super Capacitor

SLG Single Layer Graphene

ta-C Tetrahedral Amorphous Carbon

TEM Transmission Electrical Microscopy

Introduction

Carbide derived carbon, also called CDC, is a carbon based nano-scale porous material, synthesized from carbides such as SiC and TiC.[1]. CDCs can be formed by several methods, including halogen etching[2], reaction between calcium carbide and inorganic salts[3], hydrothermal treatment[4], thermal decomposition of carbide in vacuum environment[5]. Most of the methods are under high temperature or using hazardous materials like chlorine gas. CDCs can also be synthesized by electrolysis[6]; a carbide substrate is immersed in molten salt under controllable voltage.

In this study, CDC is made from Titanium carbide in LiCl-KCl molten salt. Theoretically, no chlorine could be produced during this process. Also, the level of this synthesis process may be controlled by the voltage applied by a power source. And because of the thermal properties of LiCl-KCl eutectic, this method could work in a lower temperature compare to those methods above.

Literature review

2.1 Molten salts electrolysis

Molten salt means liquid inorganic salts. The most common molten salts are formed by alkali metals or alkaline earth metal with halide, silicate, carbonate, nitrate or phosphate. Molten salt is usually used in temperature which a little bit higher than its crystallization point, because of the similar structure between melt and solid in this temperature and the properties are similar. However, there are also some difference between solid and melt. For example, the degree of disorder in crystal is increased in molten salt, so the conductivity of molten salt is higher than solid[7].

Because of the advantages of molten salt electrolysis like high conductivity and low concentration polarization, this method is widely used in chemical, metallurgy, and the plating industry[8].

The disadvantages of this method, are the high corrosive properties, especially for chlorides. The products made by this process, like chlorine, are corrosive, so higher quality of equipment is required. Also, highly volatile electrolyte, and large need of power are disadvantages of this method.

2.2 Introduction of carbon

Carbon has many superiorities: high strength, low density, high heat, corrosion and radiation resistance, high stiffness, high conductivity[9]. Today, carbon materials are developing rapidly.

In a long period, people focused on three allotropes of carbon. Graphite is a good solid lubricant, because of its layered structure. Diamond has network covalent structure, make it the hardest material in nature. In 1985, Kroto H.W et.al found that carbon element could be formed by 60 or 70 carbon atoms[10]. In 1991, Iijima S et.al, found nano-scale multilayer tubular by using high resolution TEM, which called "carbon nanotube (CNT)", also called "Bucky tube"[11].

2.3 Carburization methods

Carburization is a heating process to improve the surface strength and wear resistance for metal. Metal absorbs carbon during this process, usually higher temperature and longer processing time increase the thick of carbon film on the surface[52].

There are three typical methods for carburization: gas carburizing, liquid carburizing and solid carburizing. The most common method is gas carburizing, CO is used in gas carburizing process for common. Thomas et.al studied 316 stainless steel processed by low-temperature gas carburizing. They found the residual compressive

stress of the sample is high, up to 2.7GPa[53]. Gas carburizing is the most effective carburization method, compare with liquid and solid carburization.

For Ti alloy, A.F.Saleh et.al studied Ti–6Al–4V carburization by using laser melting. A CO2 laser, with 3kW power, is used in their study, and TiC crystals are found on the surface of sample[54].

CO is easy to form TiO on the surface of Ti alloy, so gas carburization is hard to use for Ti alloy carburization. And the cost of high energy beam equipment is high. Because of these reasons, solid carburization is a feasible method for Ti alloy carburization. Ziyuan Zhao et.al use solid carburization by cast iron to fabricate TiC coatings, the thickness of coating is over 23μm[55]. The schematic is shown in Fig 2.1:

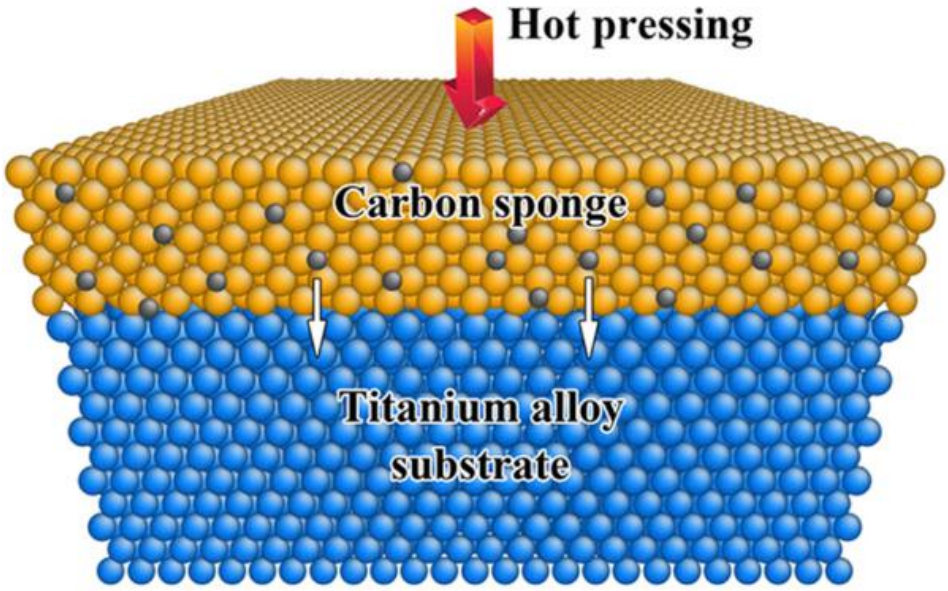

Fig 2.1 Schematic of solid carburization for Ti alloy[55]

2.4 Synthesis of Carbon Derived Carbide

Most carbon structures, including amorphous and nano crystalline graphite, CNTs, nano diamond, could synthesized from metal carbides. The microstructure, pore shape and pore size of products can be controlled by adjusting parameters and composition of the primary carbide. During past decades, synthesis of CDC was well developed.

2.4.1 Synthesis of Carbon Derived Carbide by Etching in Halogen Gas

Halogen gas (chlorine gas for example) can be used to produce CDC under high temperature. The mechanism of this method is that atom of metal can be removed from carbide, by forming tetrachloride with chlorine gas. This method was invented in 1918 by Hutchings et.al. for preparing silicon tetrachloride[19]. The reaction equation shows in equation 2.1:

$$\mathbf{SiC} + \mathbf{2}\boldsymbol{Cl_2} = \boldsymbol{SiCl_4} + \boldsymbol{C} \qquad (2.1)$$

Mohun et.al found that after removing metal atoms and surplus chlorine gas, there is an unknown type of carbon inside, they call it “the fourth category amorphous carbon” [20]. Fedorov et.al studied the porous structure and absorbability of CDC systematically. They concluded the mechanism by analyze the TiC, NbC, VC, MoC, ZrC etched by chlorine gas[21], the mechanism is shown in equation 2.2:

$$\mathbf{MC} + \frac{\boldsymbol{x}}{\mathbf{2}}\boldsymbol{Cl_2} = \boldsymbol{MCl_x} + \boldsymbol{C} \qquad (2.2)$$

When M = Ti and Zr, x=4, when M = Niobium, x=5.

For some carbides, the products are changed with temperature. They also studied the influence of different halogen by using their thermodynamic model and estimate the influence of parameter during the process, this model was used in several carbides. Research shows that TiC, SiC, Ti_2AlC and Ti_3SiC_2 can used to synthesis CDC by chlorination[22-27]. The necessary Gibbs free energy and temperature for chlorination of some kinds of carbide is shown in Table 2.1:

Table 2.1 Demands of chlorination of carbides

Carbide	GFE(kJ/mol)	Chlorination Temperature(℃)	Reference
SiC	$SiCl_4$: —505.3	~800	[22]
Ti_3SiC_2	—	~500	[23]
TiC	$TiCl_4$: —618.6	~400	[24]
B_4C	BCl_3: +27.7	~600	[25]
ZrC	$ZrCl_4$:-732.7	~400	[26]
NbC	—	~700	[27]

Nicolas Bastisse et.al studied synthesis CDC by using fluorine gas[28]. They use fluorine and xenon fluoride react with SiC to produce nanostructure carbon film. Results shows that using fluorine gas can synthesis CDC from Si at lower temperature compared with chlorine gas; When SiC was etched directly by fluorine gas, the carbon film contain SiC remains; However, when SiC was etched indirectly by xenon fluoride, the carbon film would not contain SiC remains.

2.4.2 Synthesis of Carbon Derived Carbide by Calcium Carbide React with Inorganic Salts

CDC can be synthesized by reaction of inorganic salts and calcium carbide at high temperature, and some by-products would form in this process [29, 31]. Normally, this reaction is considered as exchange reaction of calcium carbides and metal salts in high temperature. This method was first used to synthesis graphite[30]. The mechanism is shown in equation 2.3-2.5:

$$\mathbf{Ca}C_2 + MgCl_2 = MgC_2 + CaCl_2 \quad (2.3)$$

$$2MgC_2 = Mg_2C_3 + C \quad (2.4)$$

$$Mg_2C_3 = 2Mg + 3C \quad (2.5)$$

Exchange reaction and thermal decomposition reaction are both happened during this process. The reaction temperature for this reaction is 800-1275℃ for 1-5 hours. The yield of amorphous carbon up to 85%, graphite and CNT also exist in product.

Fedorov et.al studied porous structure and adsorptive property of CDC synthesized by reaction of calcium carbide and sodium chloride [32]. This process works in 400-900℃，and the reaction as shown in equation 2.6:

$$\mathbf{Ca}C_2 + 2NaCl = 2C + 2Na + CaCl_2 \quad (2.6)$$

The detail of this process: Calcium carbide and sodium chloride are mixed; the mix ratio is 1: (1-3) and sealed under 5-40MPa. The mixture is heated up to 600-1000℃ in inert environment. The production is cleaned by water and acid, then dried and crushed.

2.4.3 Synthesis of Carbon Derived Carbide by Supercritical water filtration

Gogotsi et.al found carbon coatings on SiC substrate after they are doing selective etching in supercritical water at 300-800℃ in 100MPa. Surface of SiC fibers are smooth in 450℃, and carbon coatings are found by AES analyze[34].

Kraft et.al studied carbon formation by using CVD SiC fibers under hydrothermal conditions. The experiments were happened at 200MPa and 400-700℃ and amorphous carbon is found on the surface by using Raman spectroscopy at 650℃[35].

2.4.4 Synthesis of Carbon Derived Carbide by Thermal Decomposition of Carbides

SiC would decompose under high temperature. According to the high melting point of carbon (higher than most metals), metal would vaporize at high temperature in vacuum environment, then carbon would remain. Kusunoki et.al produced CNTs in vacuum environment by thermal decomposition method. β-SiC sample was heated rapidly to 1700℃ by laser beam and CNTs was observed by TEM[36].

Euler F et.al found that silicon carbide could decompose at 2000℃ in vacuum environment and generate carbon[37]. Iijima S. studied the thermal decomposition of SiC by vacuum electron beam, graphite was found in production[38]. Foster L M et.al produced graphite by thermal decomposition of aluminum carbide; aluminum carbide was decomposed at 2400℃ in protection of argon[39].

2.5 Structure of Carbon derived carbide

The structure of Carbon derived carbide has been studied during past decades. Sascha Welz et.al studied the carbon structures in SiC CDC by transmission electron microscopy (TEM). Results show that in SiC CDC, sp^2 and sp^3 bonded carbon phase are both exist. Carbon structures in varied forms were found in this SiC CDC. And according to different processing conditions, the structure of CDC would change; amorphous carbon, graphite, diamond and spherical, polyhedral, tubular structures were found based on the parameters and position in the CDC film. Fig 2.2 shows the diagram of structures varied in CDC film.

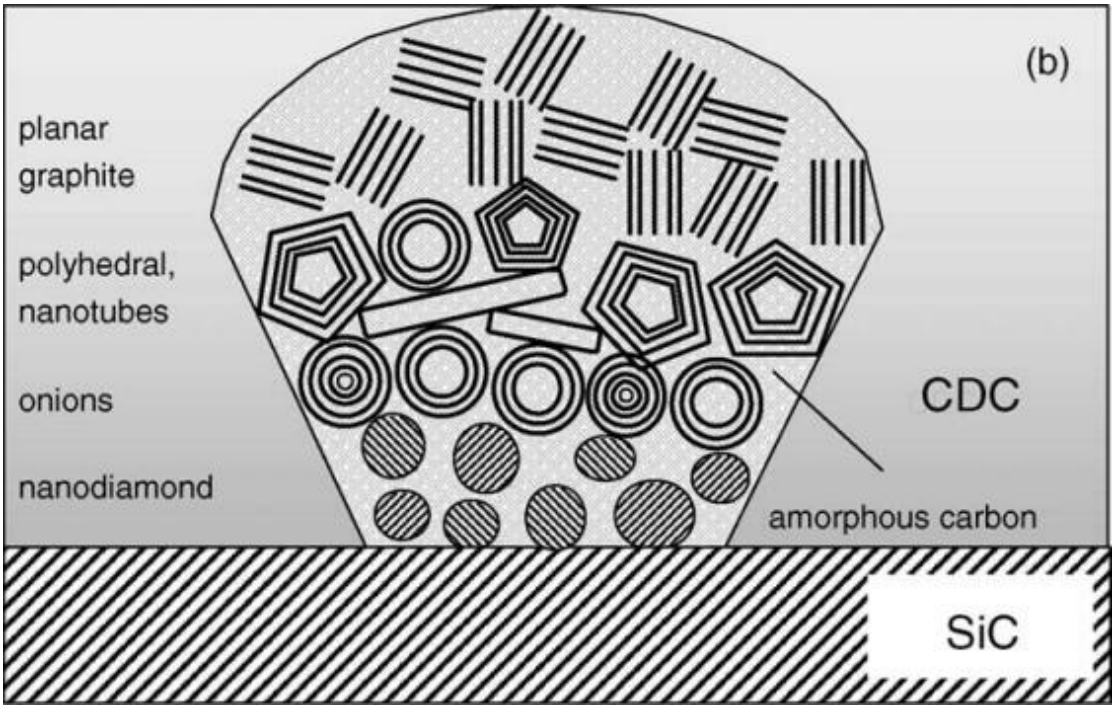

Fig 2.2 Diagram of structures varied in CDC film

Gogotsi et.al produced CDC film on SiC surface by hydrothermal method and studied the structure of CDC film. Result shows that the degree of order of carbon

increase according to the processing temperature increased, and base on this, the size of graphite crystals decreases[34].

Porosity structure is also the characteristic of CDC structure. CDC is not form by carbon deposition on the surface of substrate, however the surface of carbide is transformed to carbon. Metal components are removed from the carbide and porosity structure appeared.

Volker Presser et.al found that porous of CDC is depended on the structure of carbides. They compare the Ti_3Si_2C-CDC and SiC-CDC, results show the distribution of pore size of Ti_3Si_2C-CDC is concentrated in 0.5-4 nm, and distribution of pore size of SiC-CDC is concentrated in 0.5-1 nm. And the average size of pores increases with increasing temperature[41].

2.6 Characterizing Carbide Derived Carbons by Raman Spectroscopy

The presence of graphene-based structures such as graphite, SLGs, FLGs or CNTs can be confirmed using Raman spectroscopy. Defect-free graphene has two Raman-active peaks at 44 cm^{-1} and 1582 cm^{-1} that result from in-plane vibrations of the 2D hexagonal lattice[42]. Typically, only the 1582 cm^{-1} G-band peak is measured when characterizing graphene. Additionally, defects within graphene create a Raman-active peak at approximately 1370 cm^{-1}[42] resulting from sp2 hybridized carbon rings[33]. This peak is a result of local enhancement of a wavelength by defects rather than naturally occurring phonons within the lattice. It is also worth mentioning that the D-peak is

dependent on the presence of a ring structure. Unlike the G-band, which is a result of in-plane stretching of sp2 bonds, the D-band peak is a result of the breathing mode (in-plane, transverse, optical phonon) of rings. An excitation electron is first inelastically scattered by the incident green laser and then elastically back-scattered by defects (thereby resulting a red-shifted photon) such as sp3 bonds, vacancies, grain boundaries or edges[43].

CDC forms when the reactive element is removed from the structure leaving behind carbon that contains a mixture of sp2 and sp3 bonds without any long-range order. This amorphous carbon could be either ta-C or a-C depending on the amount of sp3 bonding. The G-band frequency of both two carbon structures is 1553 and 1565 cm^{-1}, respectively, when the excitation wavelength is 532 nm. With enough time and temperature, NCG nucleates resulting in a second G-peak forming at a frequency of 1600 cm^{-1}. Further growth of crystallites results in a down-shift in G-peak frequency until defect-free, planar graphite is formed corresponding with a G-peak at 1582 cm^{-1}When a ring structure begins to develop the D-peak becomes visible. The frequency of the D-peak depends on the size of the crystallites and the intensity is dependent upon the degree of ring formation, clustering, and as previously mentioned, the presence of defects within the rings. When deconvolution of Raman spectra results in multiple D-peak signals, the highest intensity D-peak is assigned to the G-peak with the highest degree of ordering[33].

2.7 Applications of Carbon Derived Carbide

The application of CDC is promising and wide. According to previous studies, CDC can store hydrogen and methane; CDC has low coefficient of friction and high mechanical stability; CDC can also use in supercapacitor as electrodes[47-50].

2.7.1 Supercapacitor

Supercapacitor, or SC, has great performance in pulse discharge and energy storage. Because of its great performance of great power density, better cycle life, wide using temperature and capable of multiple charge and discharge, it becomes a new type of energy storage device recently [56].

CDC can be a great choice for electrode of supercapacitor because of its porosity. As the electrode of supercapacitor, CDC can be reused over 10,000 times without any decrease of capacitance, the value of capacitance can reach 130 F/g and 115 F/cm^3 [47].

2.7.2 Storage of Hydrogen Gas

The study of storage materials for hydrogen gas is important for the application of hydrogen. There are three types of hydrogen storage mechanisms: (a) physical adsorption (e.g. porous carbon), (b) chemical absorption (e.g. metal hydrides) and (c) chemical reaction.

Carbon based porous materials are widely used in hydrogen storage because of its relative low weight, low cost, and high specific surface area[45]. Normally, the structure formed during the process which hydrogen absorbed by porous carbon materials is related to its specific surface area. However, according to some studies, other parameters like aperture also have effects[57] .

By adjusting reaction conditions during production process of CDC, different shape, size and microstructure of pores can be produced. High degree of absorption for hydrogen can be obtained by this method. Gordeev et.al[44] studied the ability of hydrogen absorption of CDC by thermal desorption-GC-MS at 300-700^{o}C under 9 times atmospheric pressure.

2.7.3 Lithium Battery

Normally, the anode of lithium battery is graphite. As anode, graphite can absorb numerous lithium ions under low voltage. S. Gautier et.al found that using ordered carbon as anode in lithium battery can get better charge capacity. The degree of order of CDC structure can be adjusted by change the reaction conditions, so CDC might be an ideal material for making the anode of lithium battery[46].

2.8 Study of mechanisms for Formation of CDC from TiC

There are several potential mechanisms working for the formation of CDC.

One is the chlorine gas can be produced during electrolysis on the sample, as shown in equation 3.1.

$$\frac{4}{x}MCl_x \rightarrow \frac{4}{x}M + 2Cl_2 \quad (3.1)$$

Then the TiC film is etched by chlorine gas, as shown in equation 3.2.

$$TiC + 2Cl_2 \rightarrow TiCl_4 + C \quad (3.2)$$

Another potential mechanism, as shown in equation 3.3, is that CDC can be produced by electrolysis in molten salt.

$$\frac{4}{x}MCl_x + TiC \rightarrow \frac{4}{x}M + TiCl_4 + C \quad (3.3)$$

Choice of Molten Salt and Temperature of Electrolysis

Generally, an ideal molten salt electrolysis system has these properties: high conductivity, low melting point, high chemical stability, low corrosivity to crucible and low cost. In this study, LiCl - KCl eutectic was used in process.

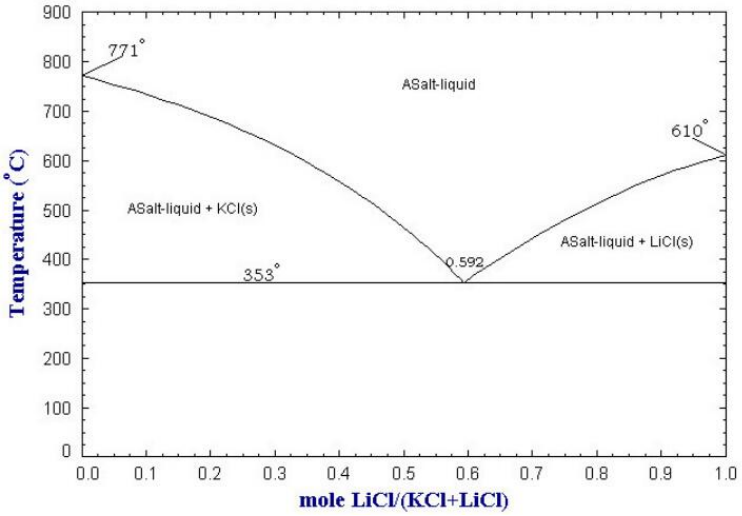

Fig 3.1 LiCl-KCl phase diagram[51]

LiCl-KCl eutectic was used in this study. According to the Fig 3.1, at the eutectic point (353℃), so the electrolysis temperature is higher than 353℃. In experiments, high volatility was found when temperature higher than 500℃. So 400℃ was a proper temperature in electrolysis.

The eutectic composition of salt is 41 mol% KCl – 59 mol% LiCl. The mass proportion of KCl-LiCl as shown in equation 3.4

$$\frac{\boldsymbol{m_{KCl}}}{\boldsymbol{m_{LiCl}}} = \frac{\boldsymbol{41\% \cdot M_{KCl}}}{\boldsymbol{59\% \cdot M_{LiCl}}} \qquad (3.4)$$

Calculation of Cell Potential

The cell potential of TiC is calculated from the Gibbus Free Energy of the reaction as shown in equations 3.5 and 3.6. n is the number of transfer electrons; E is cell potential; F is the Faraday's constant.

$$\Delta \boldsymbol{G} \quad = -\mathbf{nFE} \tag{3.5}$$

$$\mathrm{E} = -\frac{\Delta \mathrm{G}^{\mathrm{O}}}{\mathrm{nF}} \tag{3.6}$$

Equation 3.7 is the relationship between value change of Gibbus free energy and temperature.

$$\Delta \boldsymbol{G_T} \ = \Delta \mathbf{H} - \mathbf{T}\Delta \mathbf{S} \tag{3.7}$$

Then,

$$\mathbf{E} = -(\Delta \mathbf{H} - \mathbf{T}\Delta \mathbf{S})/\mathbf{nF} \tag{3.8}$$

The reaction in this process is shown in equation 3.9.

$$\mathbf{4LiCl}(\boldsymbol{l}) + \boldsymbol{TiC}(\boldsymbol{s}) \rightarrow \boldsymbol{4Li}(\boldsymbol{l}) + \boldsymbol{TiCl_4}(\boldsymbol{g}) + \boldsymbol{C}(\boldsymbol{s}) \tag{3.9}$$

According to data base from NIST-JANAF, thermodynamic equation coefficients of products and reactants are shown in Table 3.1.

Process of calculation of E is shown in equation 3.10-3.12, refers to [58] and [63].

$$\begin{aligned} \Delta \boldsymbol{G_T} \ &= \boldsymbol{\Sigma}\Delta \mathbf{H}_{\boldsymbol{products}} - \boldsymbol{\Sigma}\Delta \mathbf{H}_{\boldsymbol{reactants}} \\ &\quad - \mathbf{T}\left(\boldsymbol{\Sigma}\Delta \mathbf{S}_{\boldsymbol{products}} - \boldsymbol{\Sigma}\Delta \mathbf{S}_{\boldsymbol{reactants}}\right) \end{aligned} \tag{3.10}$$

$$\begin{aligned} \Delta G_T \ = & \frac{\sum n_i A_{prod,i} T - \sum n_j A_{react,j} T}{1000} \ln\left(\frac{T}{1000}\right) + \frac{\sum n_i A_{prod,i} T - \sum n_j A_{react,j} T}{1000} \\ & - \frac{\sum n_i B_{prod,i} T^2 - \sum n_j B_{react,j} T^2}{2 \times 10^6} - \frac{\sum n_i C_{prod,i} T^3 - \sum n_j C_{react,j} T^3}{6 \times 10^9} \\ & - \frac{\sum n_i D_{prod,i} T^4 - \sum n_j D_{react,j} T^4}{12 \times 10^{12}} - \frac{\sum 500 n_i E_{prod,i} - \sum 500 n_j E_{react,j}}{T} \end{aligned}$$

$$+\sum n_i F_{prod,i} - \sum n_j D_{react,j} - \frac{\sum n_i G_{prod,i}T - \sum n_j G_{react,j}T}{1000} \quad (3.11)$$

$$E = \frac{\Delta G_T^o}{nF} \quad (3.12)$$

Table 3.1 Thermodynamic equation coefficients[63]

compound	Temperature(K)	Shomate Equation Coefficients
TiC(s)	298 to 1000	A=5.554, B=149.865, C=-171.069, D=67.135, E=-0.269, F=-191.942, G=-8.253, H=-184.096
KCl(l)	1044 to 2000	A=73.596, F=-443.734, G=175.720, H=-421.793
LiCl(l)	883 to 2000	A=73.180, B=-9.0472, C=-0.316, D=0.079, E=0.014, F=-417.131, G=157.671, H=-390.756
$TiCl_4$(g)	500 to 1100	A=104.779, B=6.897, C=-5.533, D=1.598, E=-1.019, F=796.809, G=474.223, H=-761.892
C(s)	500 to 1500	A=6.759, B=29.778, C=-18.372, D=4.192, E=-0.741, F=-5.5193, G=2.096, H=0
Li(l)	453 to 700	A= 32.470, B=-2.637, C=-6.327, D=4.230, E=0.006, F=-7.117, G=74.294, H=2.380
K(l)	336 to 1040	A=40.271, B=-30.545, C=26.495, D=-5.728, E=-0.063, F=-8.812, G=127.761, H=2.271
Cl_2	298 to 1000	A=33.505, B=12.229, C=-12.065, D=4.385, E=-0.159, F=-10.835, G=250.029, H=0

The results of decomposition voltage at 400℃ are shown in Table 3.2.

Table 3.2 Cell potential at 400℃

Mechanism	Reaction	Cell potential/V
(3.1), (3.2)	$2LiCl \rightarrow 2Li + Cl_2$	-3.8
	$2KCl \rightarrow 2K + Cl_2$	-3.9
(3.3)	$4LiCl(l) + TiC(s) \rightarrow 4Li(l) + TiCl_4(g) + C(s)$	-2.3
	$4KCl(l) + TiC(s) \rightarrow 4K(l) + TiCl_4(g) + C(s)$	-2.4

The results here are calculated in theoretic environment and with the data from [63]. The results here show that the cell potentials of reactive anode synthesis are lower

than the cell potentials of electrolysis of the electrolyte to form chlorine gas[58], which means reactive anode electrolysis is the lower energy path in LiCl-KCl salts.

Experiment

Mechanism

Molten salt electrolysis is used in this experiment to make CDC. Ti-6Al-4V sample with TiC film on the surface is used as substrate and anode, LiCl and KCl are set in a Ni crucible. The potential reaction mechanism is shown in equations 4.1

$$4\mathrm{Li}Cl(l) + TiC(s) \rightarrow 4Li(s) + TiCl_4(g) + C(s) \quad (4.1)$$

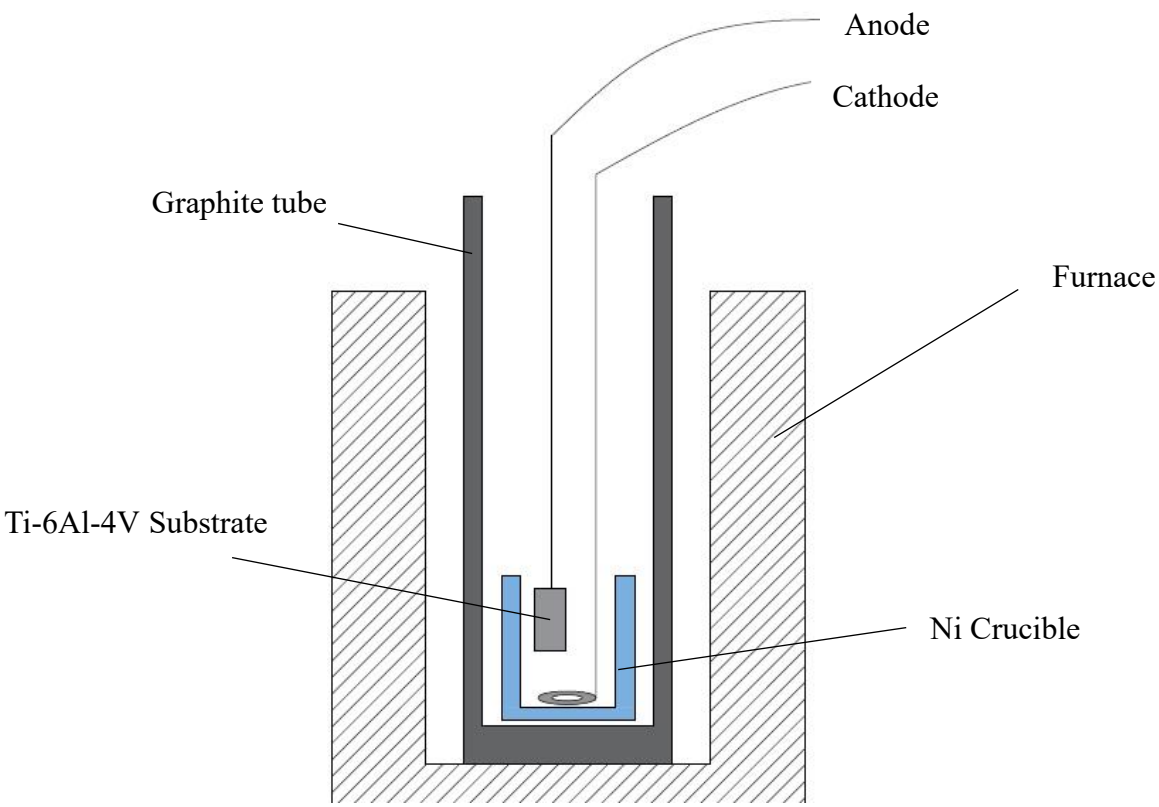

Fig 4.1 Reactor

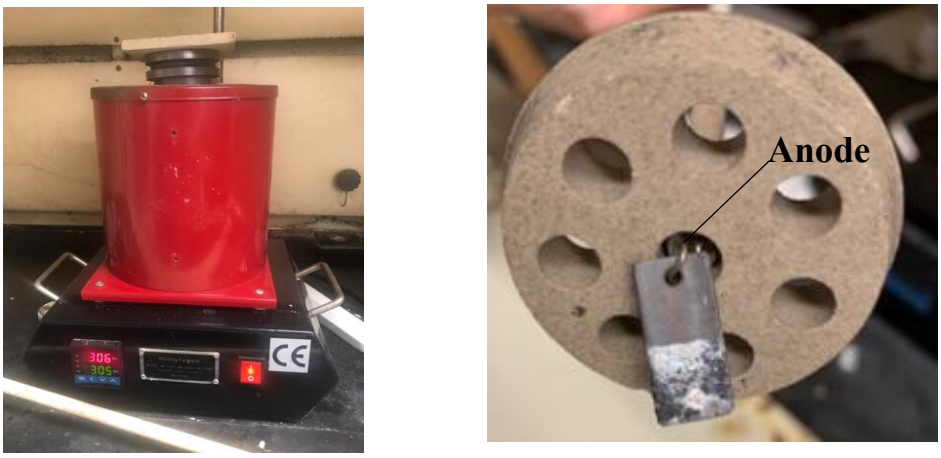

Fig 4.2 Image of furnace and sample

Preparation of reactor and crucible

The experiments were carried out in a device as shown in Fig.4.1, a graphite tube set in a furnace. In the bottom of tube is a Ni crucible, the dimensions of this crucible are shown in table 4.1, with 24g LiCl and 33g KCl powder in it. Dry the system in 300℃ for 2 hours in order to take the moisture out. Because of the melt point of LiCl-KCl eutectic is around 353℃, heat the crucible up to 400℃ for 30 minutes to melt the salts. Thermocouple is used to check the temperature of molten salts before the experiment start.

Table 4.1 Dimensions of Ni crucible

Product No.	Capacity	Height	Top Diameter	Wall Thickness
847-50NI	50ml	48mm	44mm	0.75mm

Sample was tied by an electrode, as anode, fixed on a ceramic tube to position it in the center of the crucible filled with molten KCl-LiCl. Sample should be held carefully during experiments, to make sure it can be well submerged by molten salt. A coil with Ni wire is fixed at the bottom of crucible, as shown in Fig 4.1.

Preparation of samples

Solid state carburization under an inert gas environment is used to produce TiC film on the surface of the metal substrate. A Ti–6Al–4V substrate is covered by 99% graphite powder. In order to get better result, press a block above the graphite powder to make it more compact, as shown in Fig 4.3. Then the Ti–6Al–4V substrate is heated at 1000℃ purged with Ar gas for 24 hours in furnace, as shown in Fig 4.5. Carbon reacts with Ti to form TiC at the interface between the two reactants and the TiC layer grows into the metal surface. The result expected is shown in Fig 4.4.

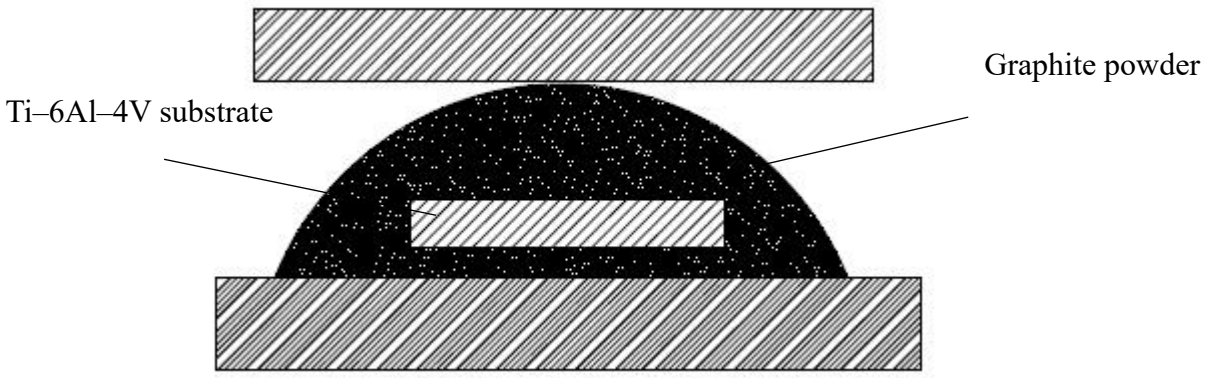

Fig 4.3 Ti–6Al–4V substrate covered by graphite powder

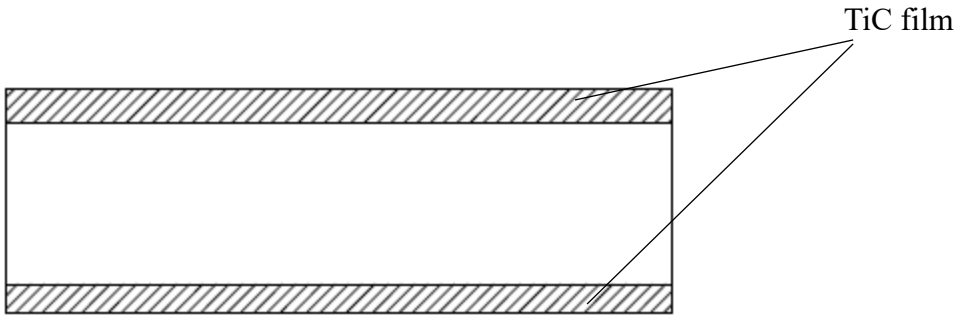

Fig 4.4 TiC film on the Ti–6Al–4V substrate

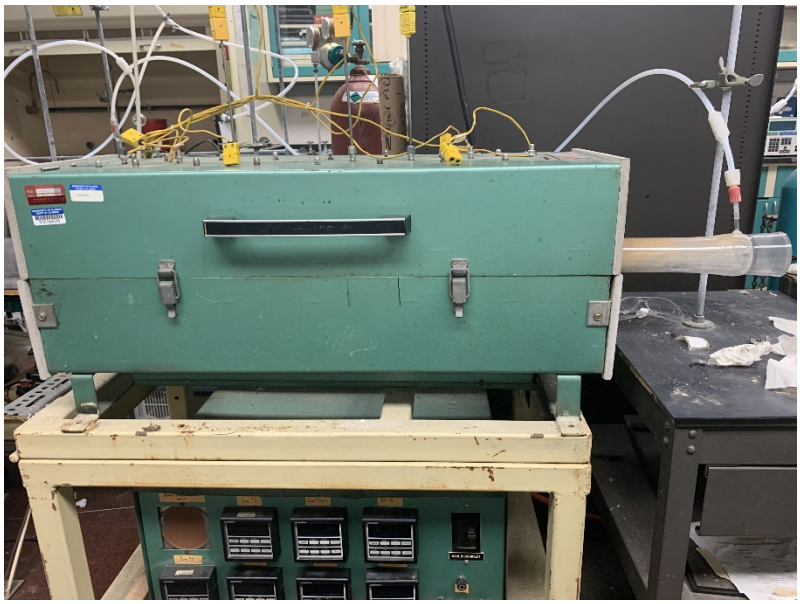

Fig 4.5 Furnace for carburization

Electrolysis Parameters

The electrolysis parameters using in this study is shown in table 4.2:

Table 4.2 Temperature, average current and voltage of reaction

Experiment	1	2	3	4	5	6
Time	1 minute					
Temperature/℃	400					
Voltage/V	2.4	2.2	1.6	1.3	0.8	0.5
Current/A	0.11	0.10	0.08	0.05	0.03	0.008

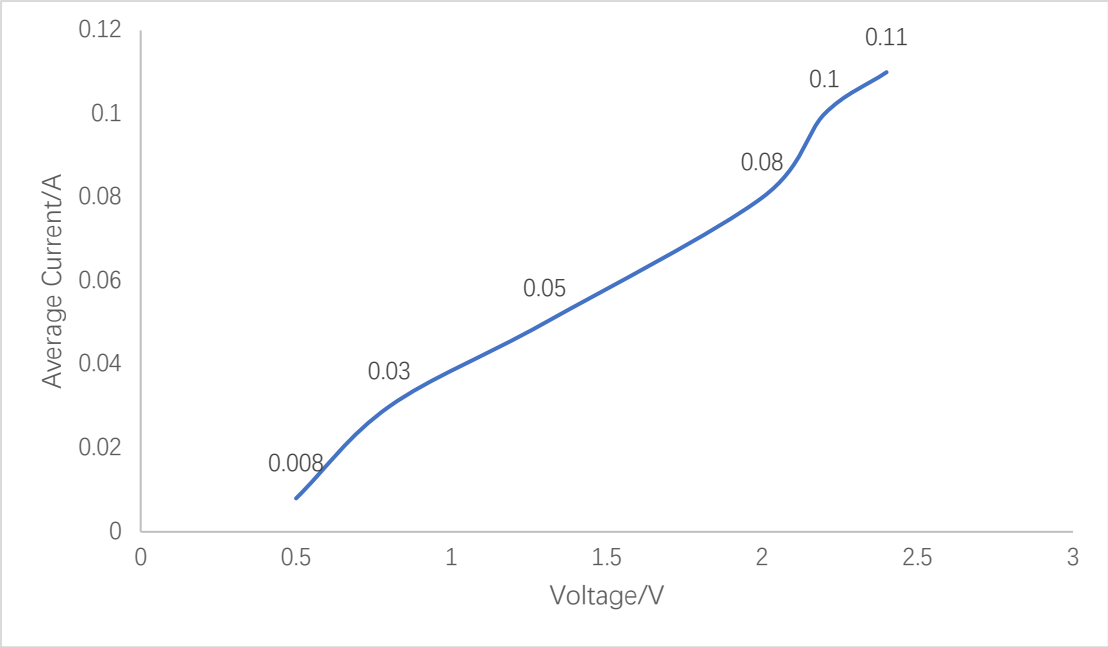

Fig 4.6 Plot of voltage – average current in experiments

Carbon Derived Carbide Characterization by Raman Spectroscopy

In order to characterize the formation of CDC on the substrate, a Renishaw InVia Raman spectrometer with 532nm green laser is used to measure the samples. Raman Spectroscopy is the most common technology to characterize carbon materials, the rotational, vibrational modes can be observed in the system. This method is sensitive to the disorder degree of structure, and the presence of graphene-based structures can be confirmed by Raman spectroscopy.

According to [33], the Raman spectra of carbon films were reviewed, including amorphous carbon. The results are listed below.

Table 4.3 Raman spectra results of carbon films

Structure	ta-C	a-C	NCG	graphite
G-peak (cm^{-1})	1553	1565	1600	1582

CDC forms when the reactive element is removed from the structure leaving behind carbon that contains a mixture of sp2 and sp3 bonds without any long-range order. This amorphous carbon could be either ta-C or a-C depending on the amount of sp3 bonding. The G-band frequency of ta-C and a-C structures is 1553 and 1565 cm^{-1}, respectively, and the excitation wavelength is 532 nm.

To study the difference of disorder under different voltage, the results are fitted and analyzed by ORIGIN using Lorentz function. The area of both D-band and G-band and two peaks are also analyzed by ORIGIN 2019, a data analysis software [59].

Results

Analysis of Raman Spectra

Each sample was divided into three parts, position1,2 and 3, as shown in Fig.5.1-5.3. In position 1, the results of Raman Spectra show relatively stable and clear. The potential reason of this phenomenon is the bottom side of samples are completely submerged by molten salt; the dotted line represents the top of the salt bath. Little electrolysis occurs in region 3 because this region is not contact with the molten salt adequately during the experiment. Also, region 2 is near the interface between molten salt and air, so the extent of electrolysis is intermittent and can vary between experiments. To compare the results of different samples, results of position 1 was chosen on every sample. And the average area of reaction region is about 0.8 cm^3.

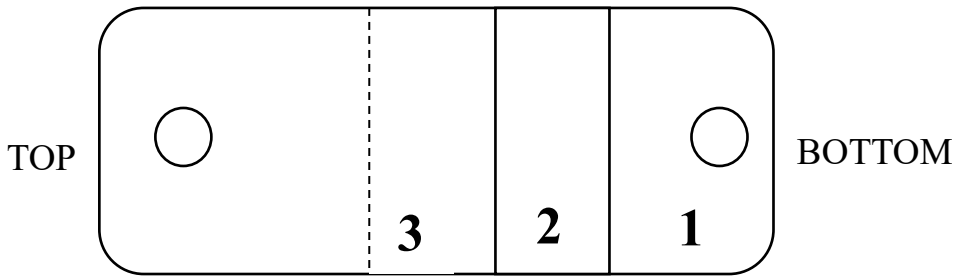

Fig 5.1 Three parts of carburized Ti-6Al-4V alloy substrate

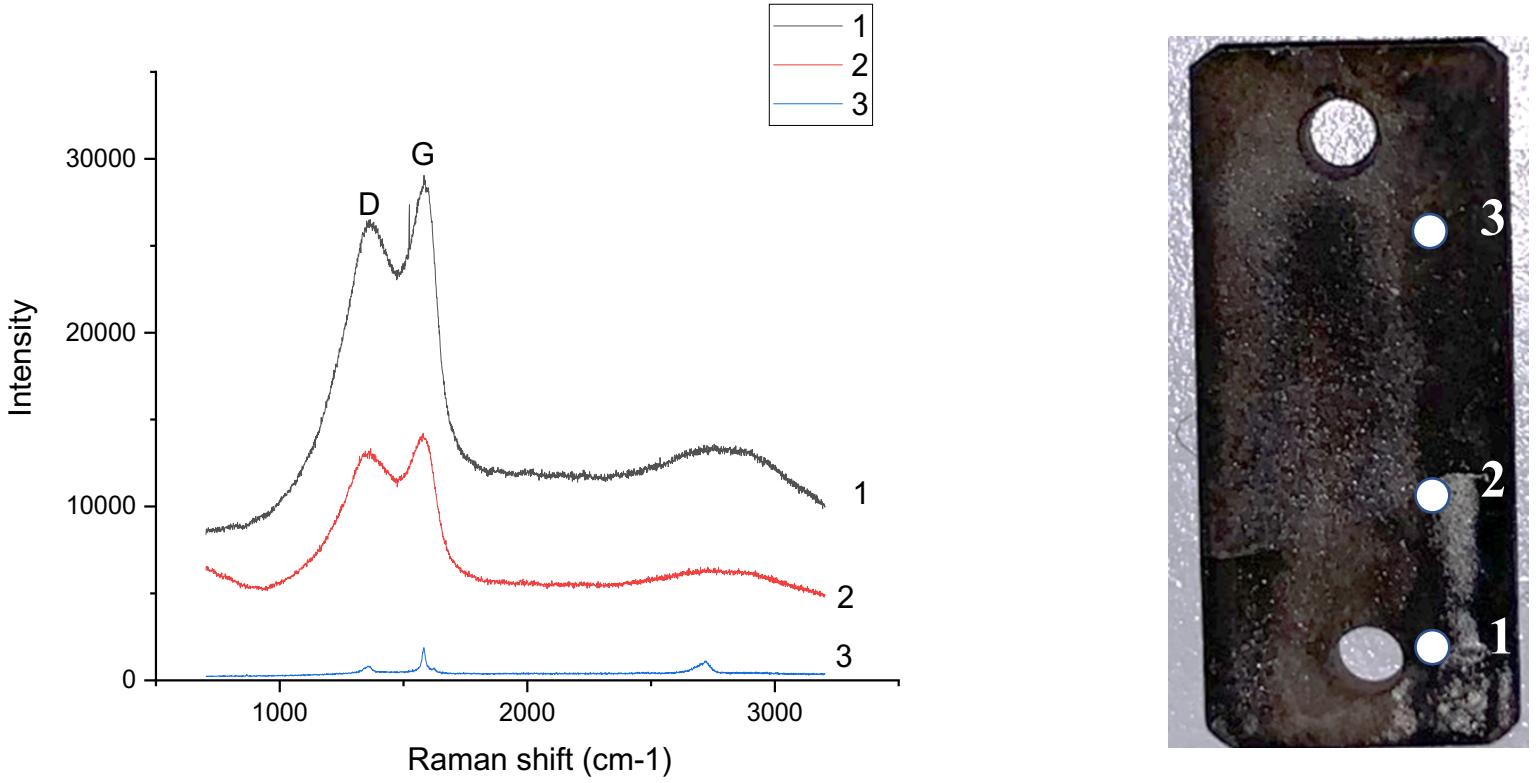

Fig 5.2 Carburized Ti-6Al-4V alloy substrate treated at 400℃ in 1 minute at 2.4V (1)Raman spectra, (2)Image of the sample

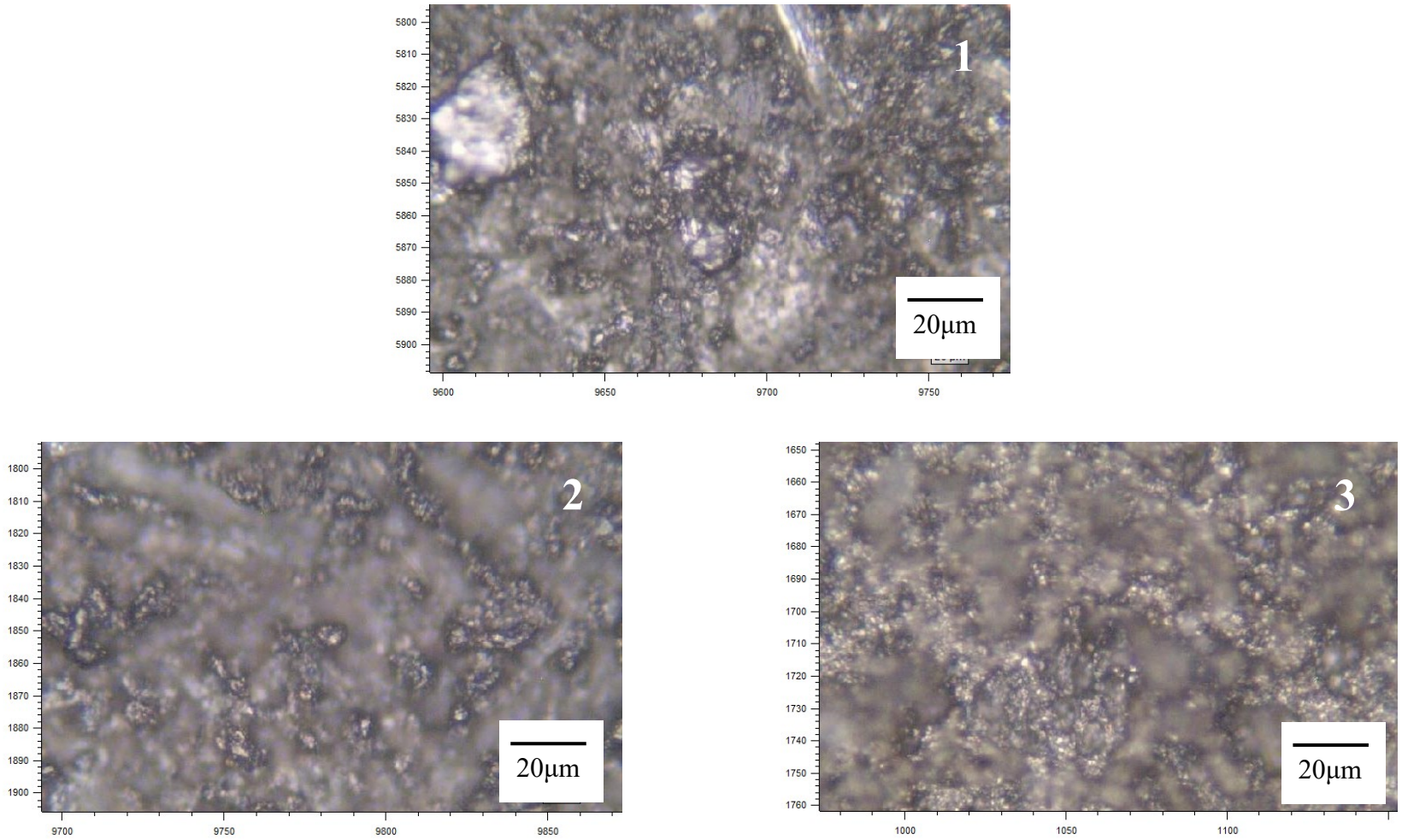

Fig 5.3 Images of position 1,2 and 3 on the surface of sample (2.4V, 1 minute, 400℃, by optical microscope)

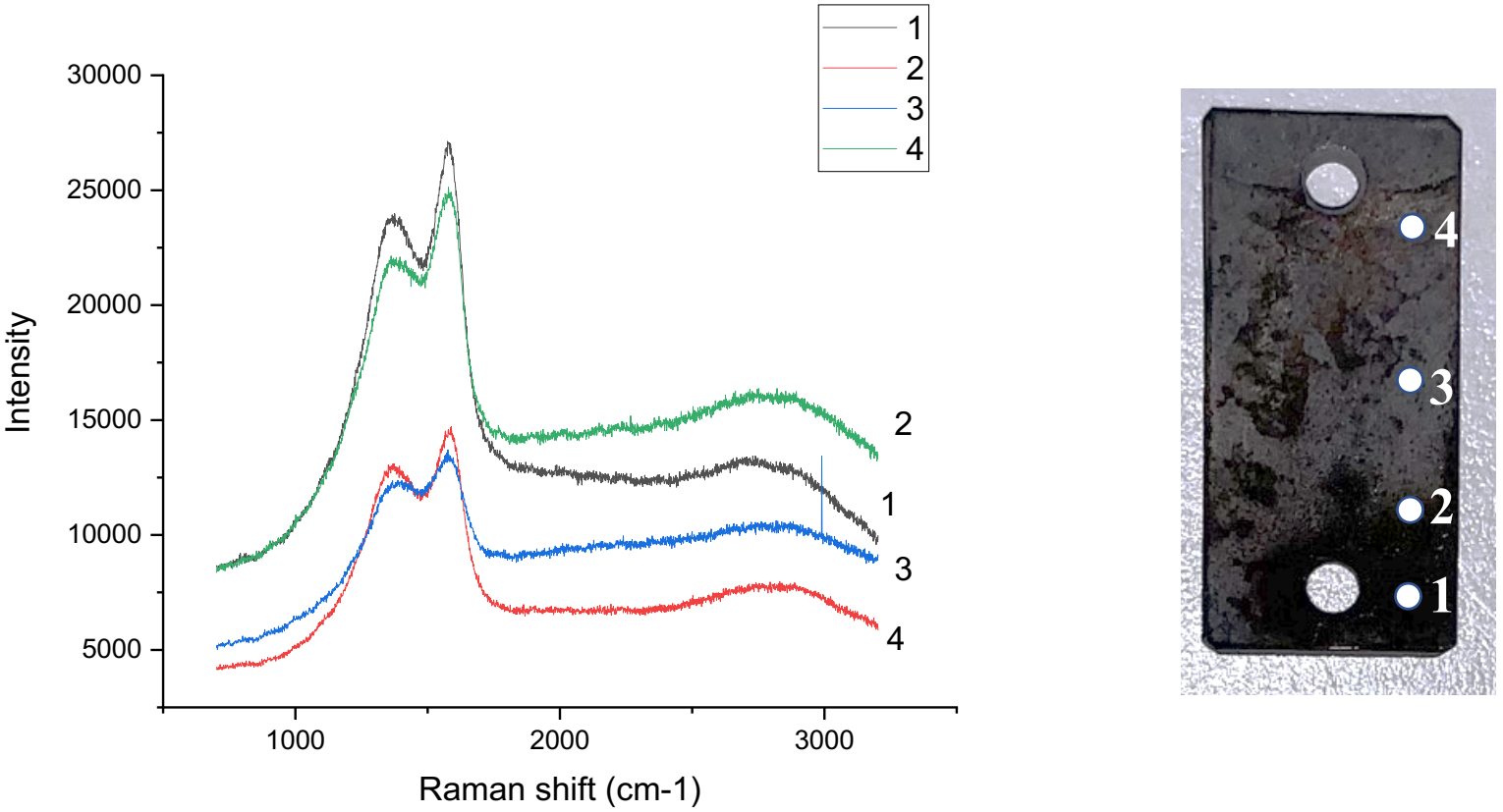

Fig 5.4 Carburized Ti-6Al-4V alloy substrate treated at 400℃ in 1 minute at 2.2V (1)Raman spectra, (2)Image of the sample

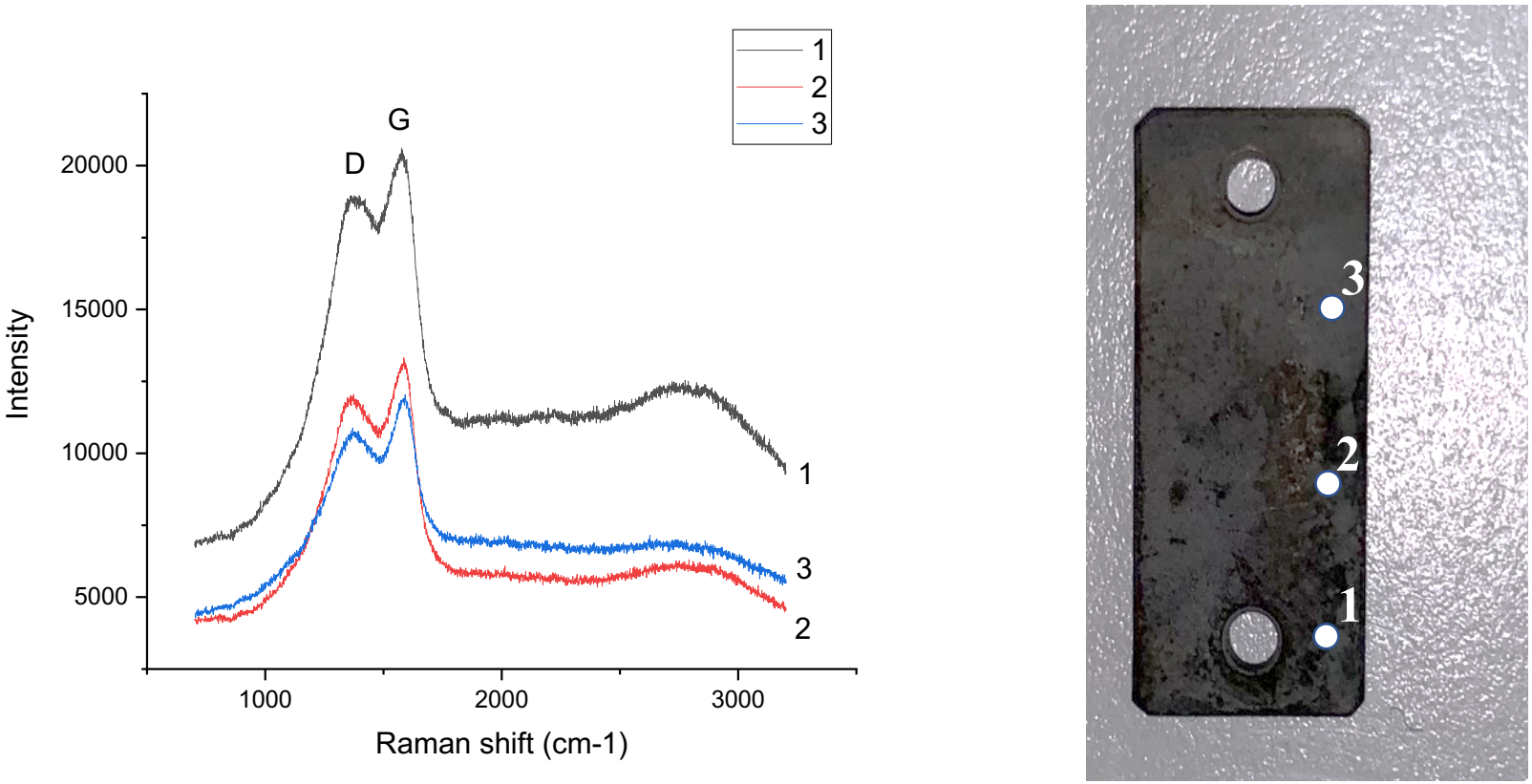

Fig 5.5 Carburized Ti-6Al-4V alloy substrate treated at 400℃ in 1 minute at 1.6V (1)Raman spectra, (2)Image of the sample

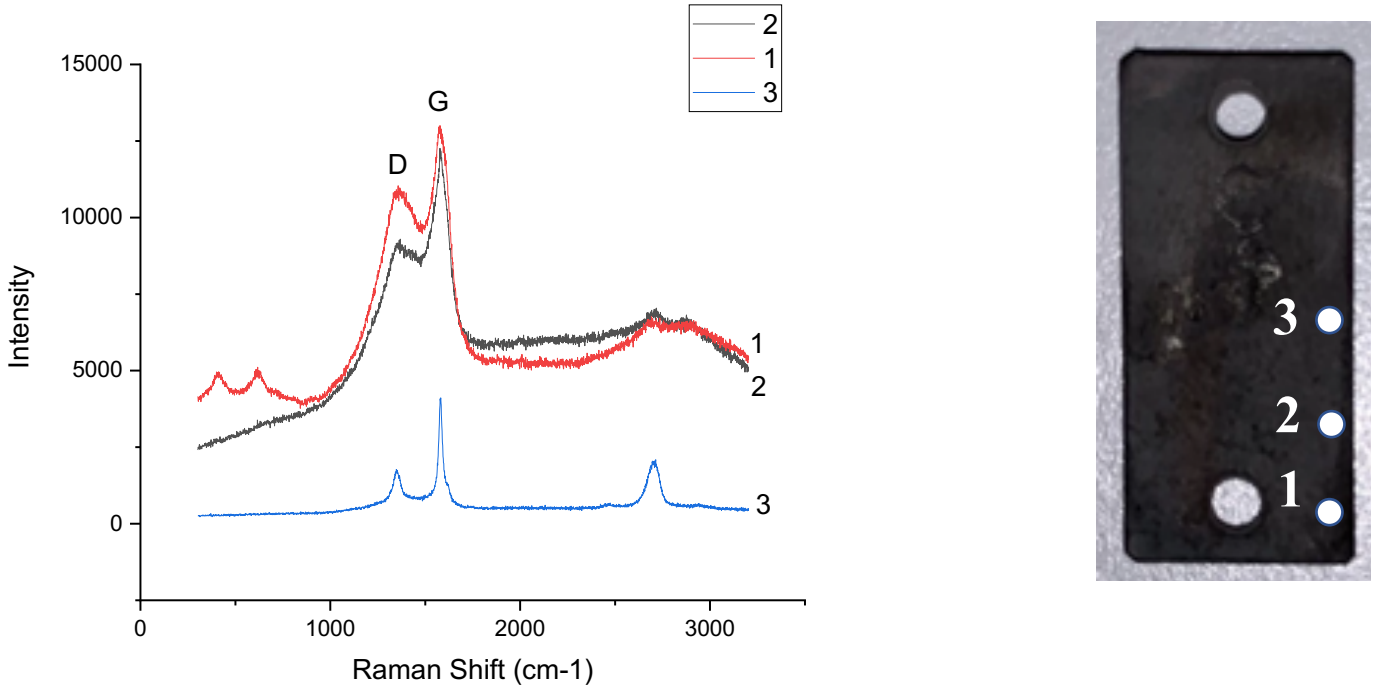

Fig 5.6 Carburized Ti-6Al-4V alloy substrate treated at 400℃ in 1 minute at 1.3V (1)Raman spectra, (2)Image of the sample

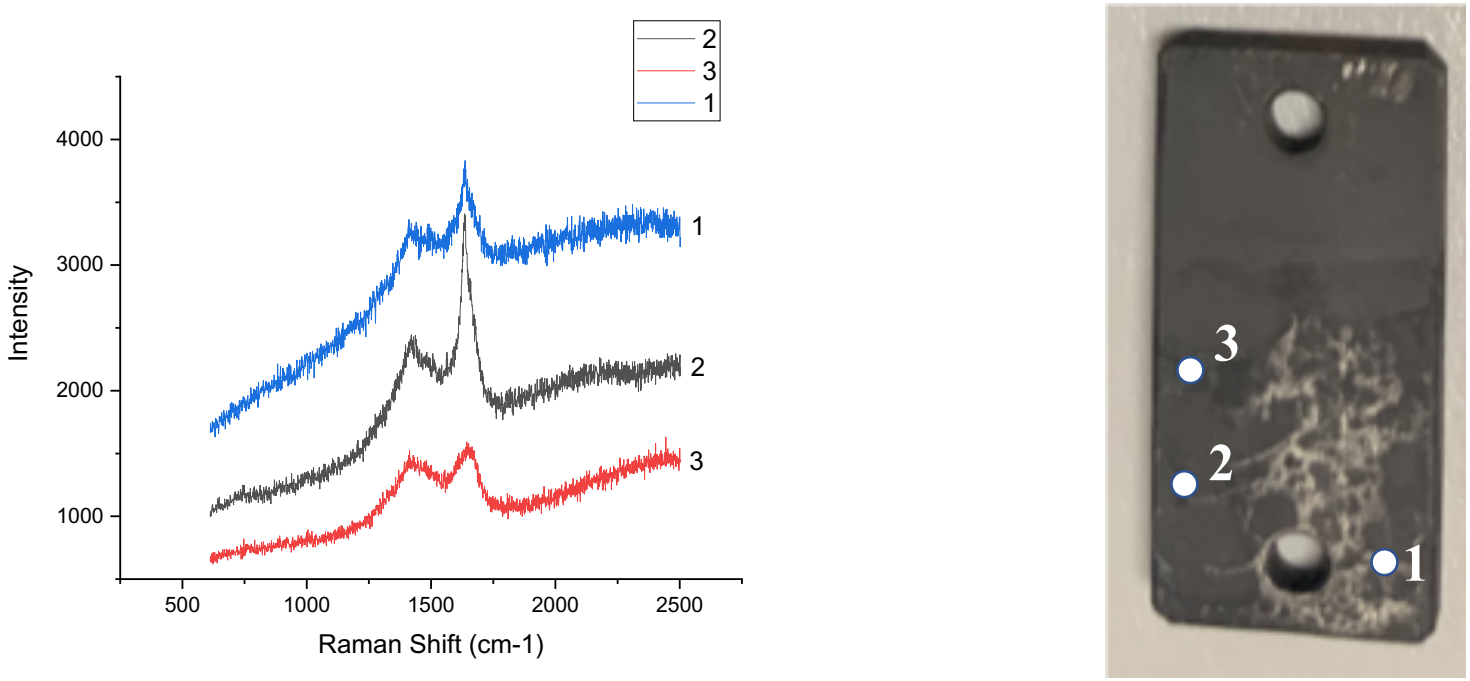

Fig 5.7 Carburized Ti-6Al-4V alloy substrate treated at 400℃ in 1 minute at 0.8V (1)Raman spectra, (2)Image of the sample

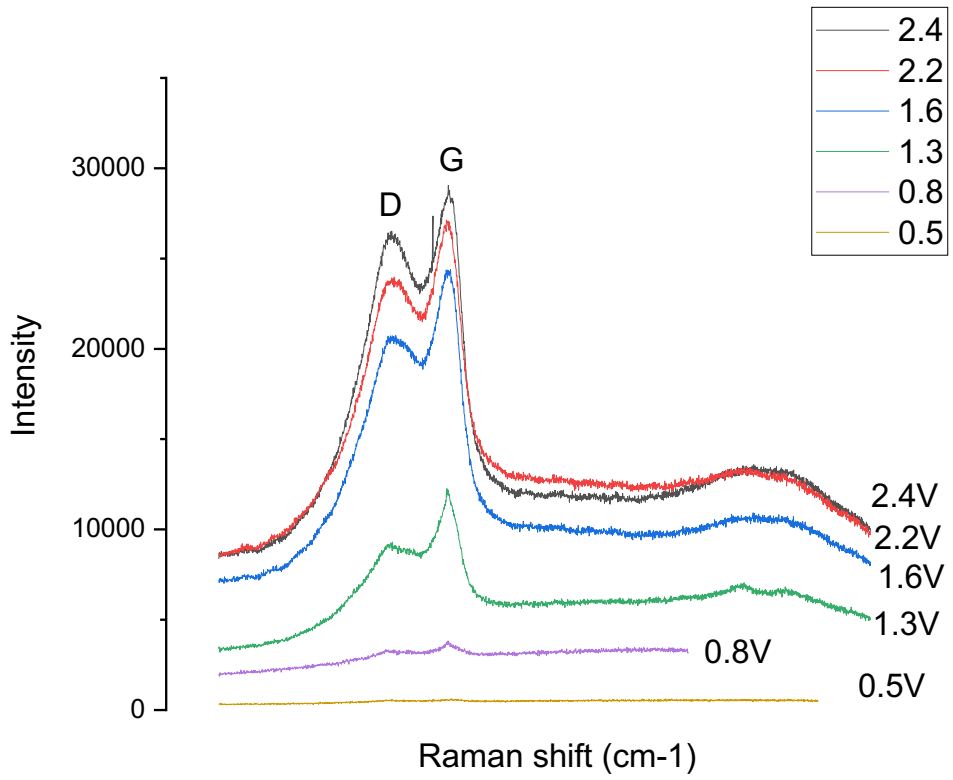

Fig 5.8 Experiment results in different voltage

Raman spectra of different TiC samples produced under different voltages in 400℃ in 1 minute are shown in Fig5.8. All spectra are taken from region 1 of the specimens, and in the range of 1000~2500 cm^{-1}, the spectra show two apparent disorder carbon peaks: D peak is 1370cm^{-1} and G peak is 1580cm^{-1}.

D peak, G peak show more separate and sharper when voltage is higher as shown in Fig5.5. In order to study this phenomenon, the ratio of intensity is estimated by ORIGIN. (Table5.9-5.14).

CDCs produced at higher voltage (1.6V~2.4V) show higher I_D/I_G, as shown in Fig 5.6, according to chapter 2.6, the D-band is associated with vibrations of sp^2 rings for excitation, which means disordered carbon materials. G-band is the result of in-plane stretching of sp^2 bonds. Changed ratio of I_D and I_G always related to graphitization [60].

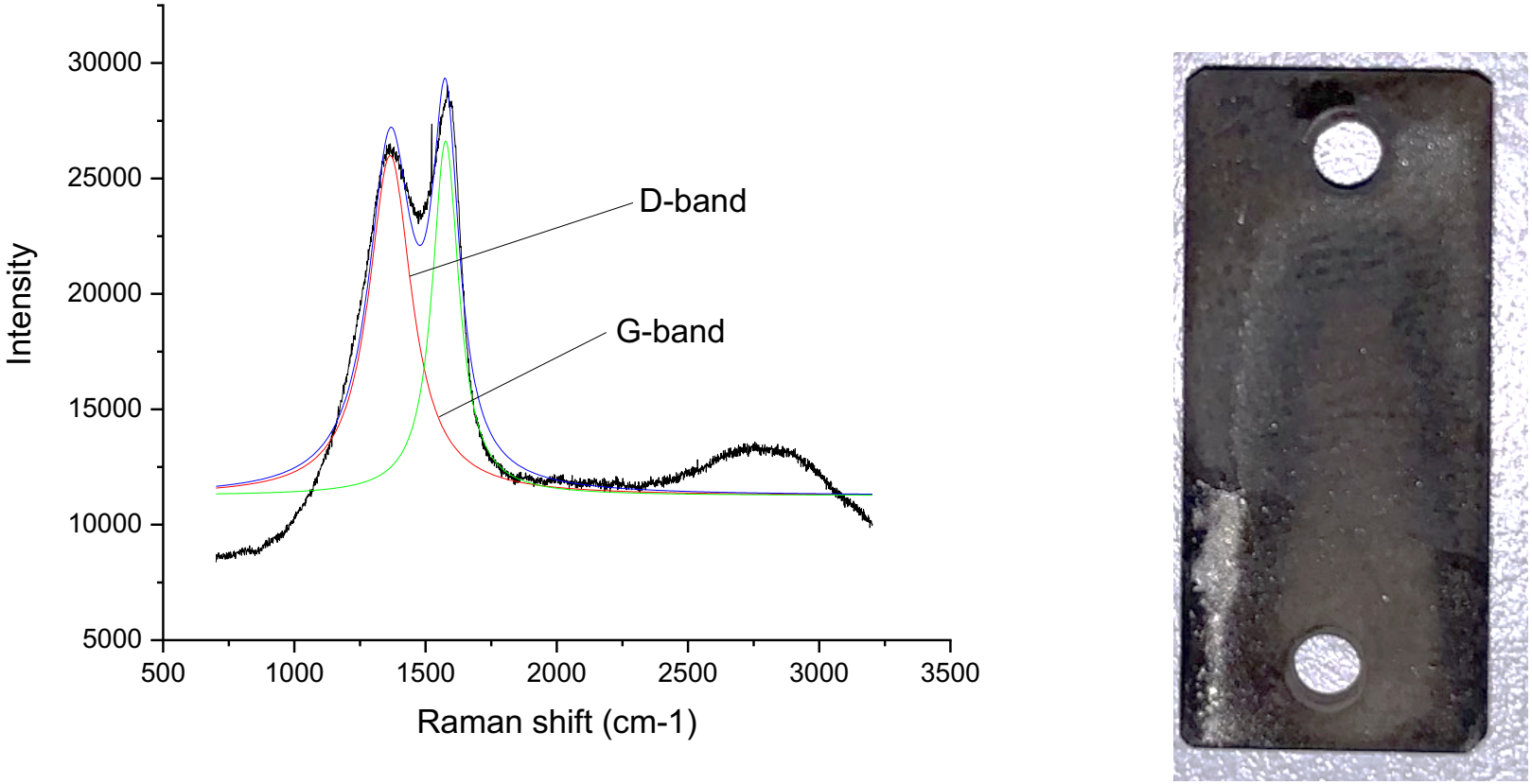

Fig 5.9 Carburized Ti-6Al-4V alloy substrate treated at 400℃ in 1 minute at 2.4V (1)Raman spectra fitted by Loreniz, (2)Image of the sample

Table 5.1 Summary of Raman results (2.4V, 1min, 400℃)

Peak	Frequency, cm^{-1}	FWHM, cm^{-1}	Height	Area	I_D/I_G
D	1365	200	14732	4538369	0.96
G	1576	123	15353	2980546	

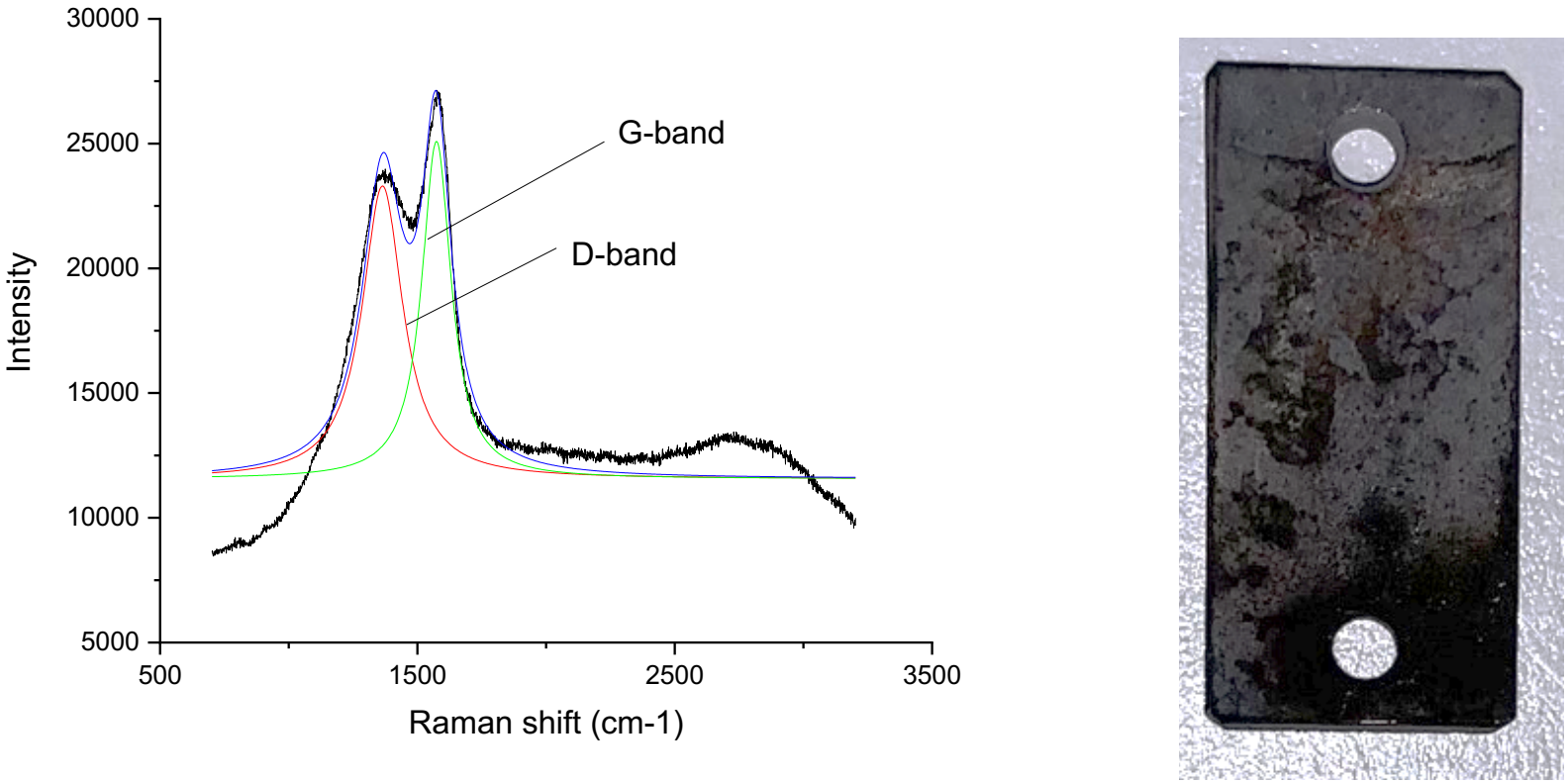

Fig 5.10 Carburized Ti-6Al-4V alloy substrate treated at 400℃ in 1 minute at 2.2V (1)Raman spectra fitted by Loreniz, (2)Image of the sample

Table 5.2 Summary of Raman results (2.2V, 1min, 400℃)

Peak	Frequency, cm^{-1}	FWHM, cm^{-1}	Height	Area	I_D/I_G
D	1364	191	11736	3530739	0.87
G	1574	137	13523	2930849	

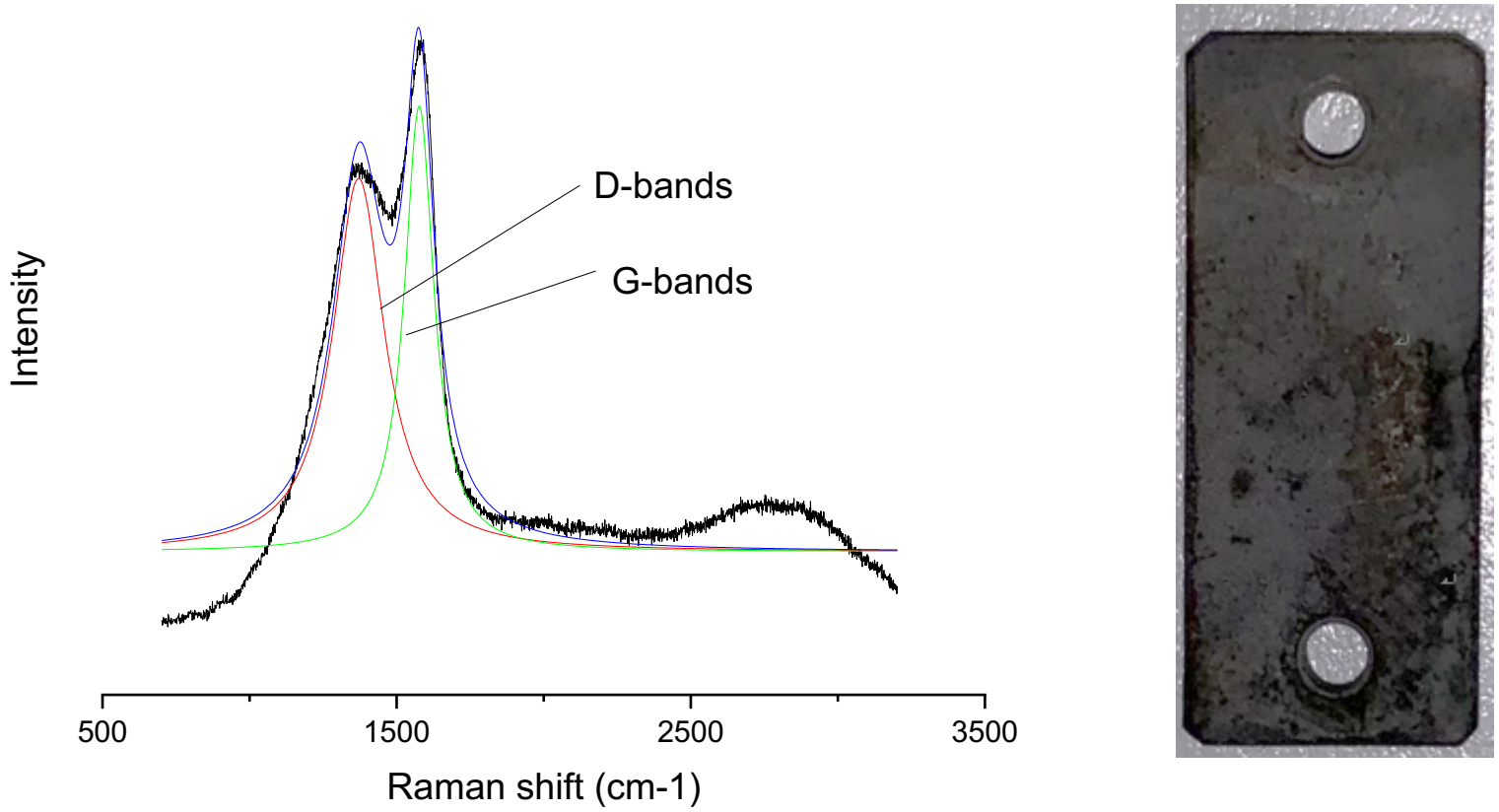

Fig 5.11 Carburized Ti-6Al-4V alloy substrate treated at 400℃ in 1 minute at 1.6V (1)Raman spectra fitted by Loreniz, (2)Image of the sample

Table 5.3 Summary of Raman results (1.6V, 1min, 400℃)

Peak	Frequency, cm^{-1}	FWHM, cm^{-1}	Height	Area	I_D/I_G
D	1370	211	11045	3671140	0.84
G	1576	121	13180	2515398	

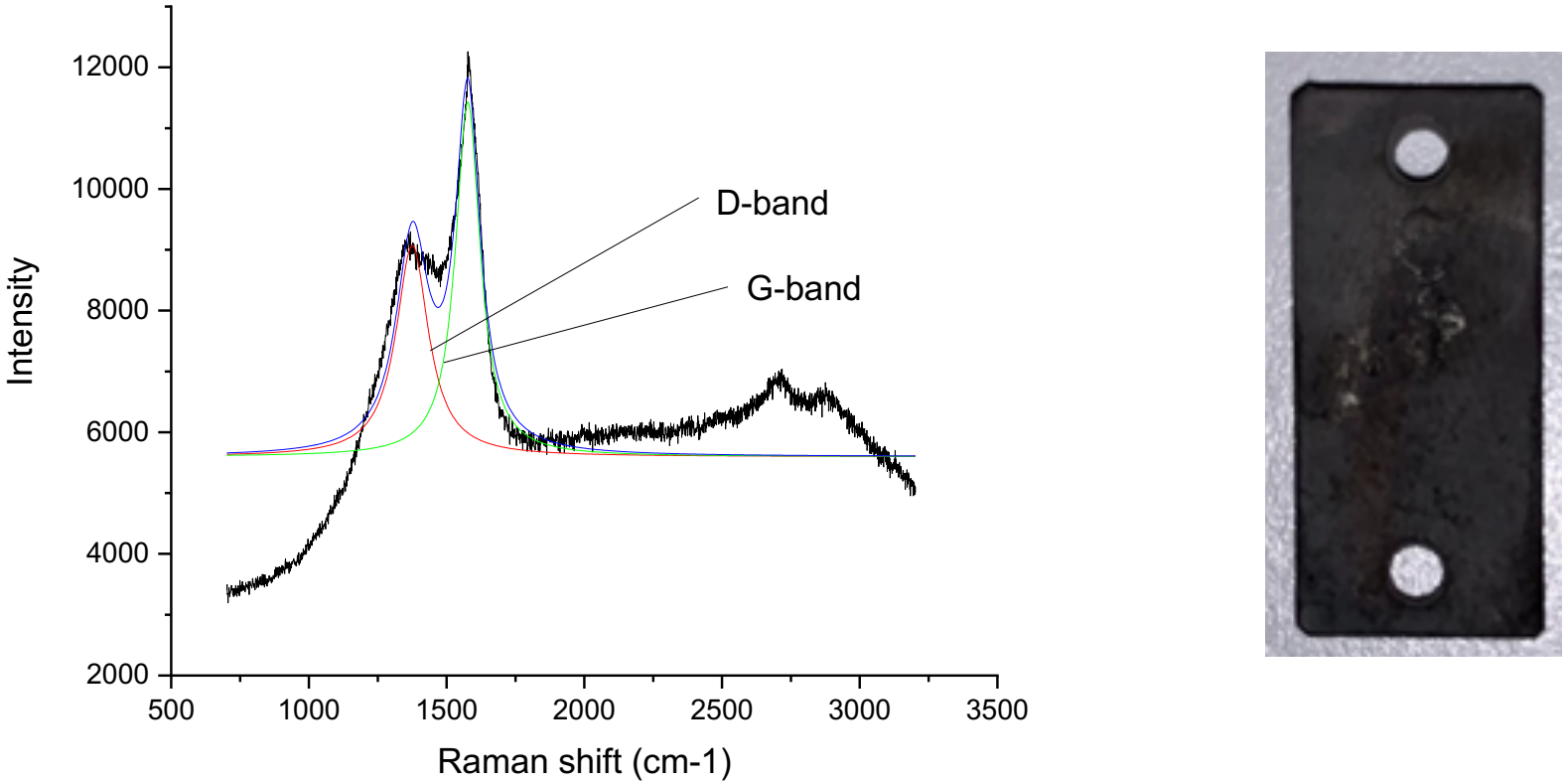

Fig 5.12 Carburized Ti-6Al-4V alloy substrate treated at 400℃ in 1 minute at 1.3V (1)Raman spectra fitted by Loreniz, (2)Image of the sample

Table 5.4 Summary of Raman results (1.3V, 1min, 400℃)

Peak	Frequency, cm^{-1}	FWHM, cm^{-1}	Height	Area	I_D/I_G
D	1375	143	3473	782326	0.59
G	1577	108	5830	990611	

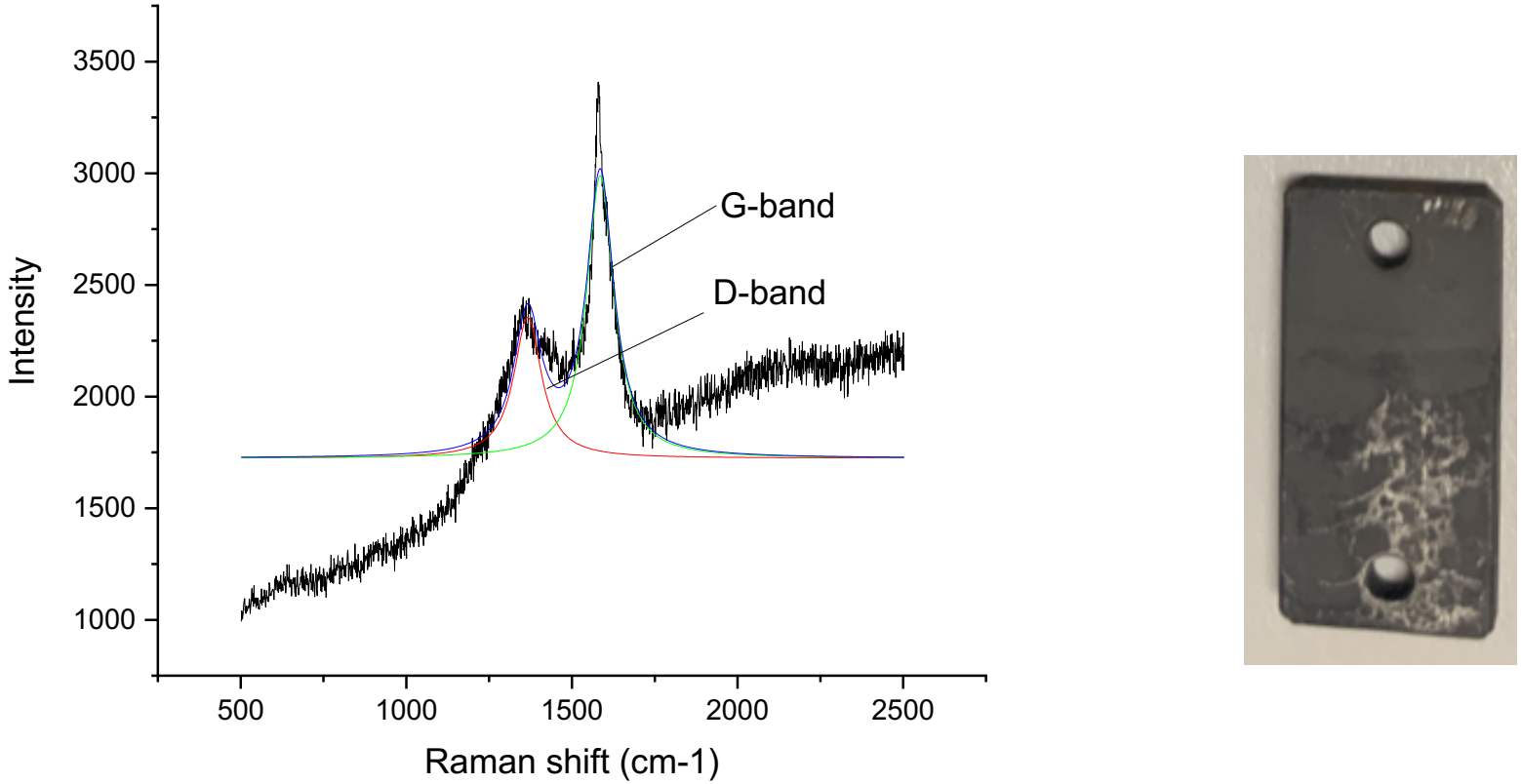

Fig 5.13 Carburized Ti-6Al-4V alloy substrate treated at 400℃ in 1 minute at 0.8V (1)Raman spectra fitted by Loreniz, (2)Image of the sample

Table 5.5 Summary of Raman results (0.8V, 1min, 400℃)

Peak	Frequency, cm^{-1}	FWHM, cm^{-1}	Height	Area	I_D/I_G
D	1366	101	630	100558	0.50
G	1585	99	1264	198330	

Fig 5.14 Corrosion on the Ni crucible

As shown in Fig 5.14, a green corrosion product was found on the surface of Ni crucible, after experiments. Most of them were found on the surface inside the crucible. Which probably means chlorine gas was created during this process and corroded the Ni crucible, $TiCl_4$ could also be corrosive and may cause this phenomenon. Another potential reason is that because of this process was exposed in air, the moisture in air may also corrode the crucible and lead it to green.

Some white crystals are found out of the graphite tube after experiments and disappeared shortly in atmosphere, as shown in Fig 5.15. These crystals supposed to be Li salt which dissolved into graphite tube and disappeared because of the moisture in open air.

The mechanisms of these phenomenon are still unknown and need to be discovered in future works.

Fig 5.15 White crystals covered the graphite tube

Discussion

Refers to Fig 4.6, the higher voltages in experiment leads to higher currents in experiments. Which means higher degree of electrolysis and more CDC formed on the surface of substrates, according to the mechanism discussed in chapter 3. And the Raman spectra results in Fig 5.8 prove could this tendency.

The relation between the ratio of I_D and I_G and voltage in experiments is shown in Fig 6.1.

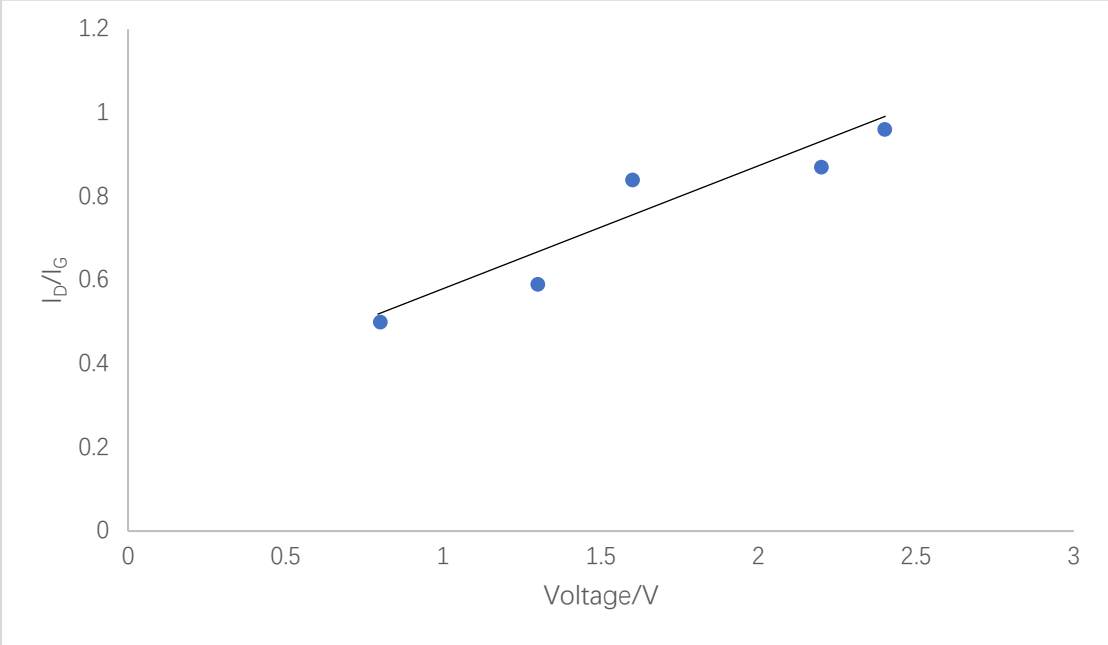

Fig 6.1 Plot of voltage – I_D/I_G in experiments

Refers to [62], the theoretical thickness of synthesized CDC can be estimated by calculation, using the data of electrolysis process. The calculation process for 2.4V experiment is shown below:

$$Q = 0.11 \times 60 Coulombs = 6.6\, Colomb/s$$

$$n_e = \frac{Q}{F}$$

$$N_c = \frac{1}{4} n_e = \frac{Q}{4F} = \frac{6.6}{4 \times 96485}\ mole = 1.71 \times 10^{-5}\ mole$$

$$M_c = 1.71 \times 10^{-5}\ mole \times 12\ g/mole = 2.05 \times 10^{-4}\ mole$$

$$\rho_c = 2.26\ g/cm^3$$

$$D = \frac{V}{A} = \frac{\frac{M_c}{\rho_c}}{A} = \frac{0.91 \times 10^{-4} cm^3}{0.8} = 1.14\ \mu m$$

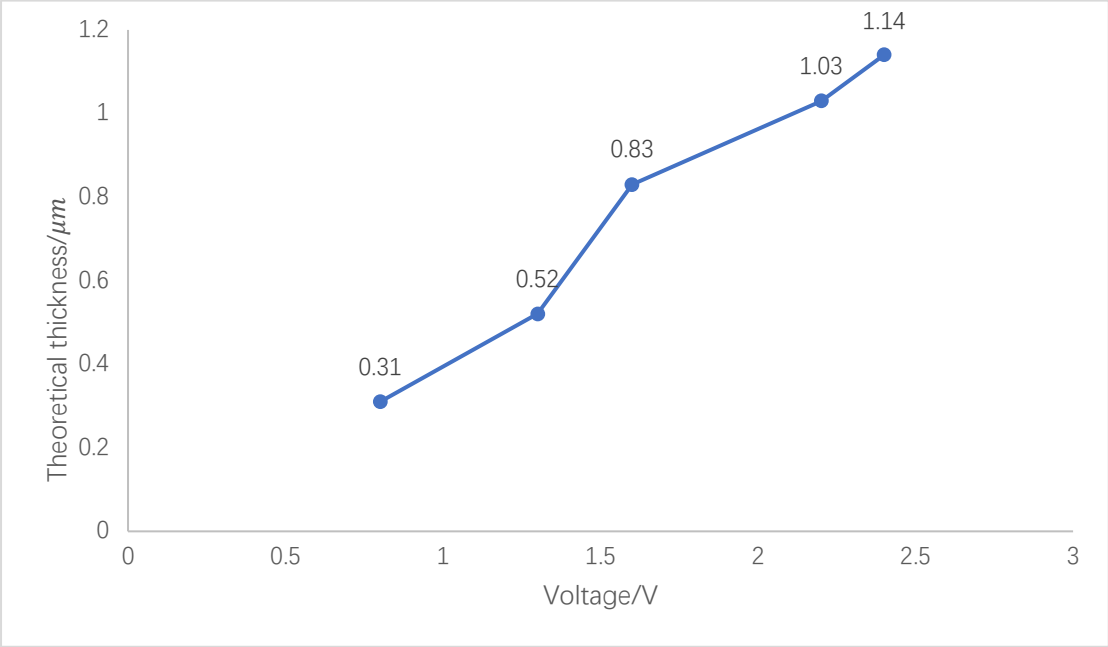

Fig 6.2 Plot of Theoretical thickness – Voltage

Refers to [58], The value of I_D/I_G represents the disorder. So, the disorder of CDC increase as the voltage increase in these experiments.

The I_D/I_G ratio can also be used to estimate the in-plane crystallite diameter otherwise referred to as the correlation length, L_a. According to [58], L_a can be estimated using equation 6.1 when $L_a > 2nm$, and can be estimated using equation 6.2 when $L_a < 2nm$, refers to [61].

$$L_a = C(\lambda)(\frac{I_D}{I_G})^{-1} \quad (6.1)$$

$$L_a = (\frac{I_D}{I_G}\frac{1}{C'(\lambda)})^{\frac{1}{2}} \quad (6.2)$$

$$\mathrm{C} = -12.6 + 0.033\lambda \quad (6.3)$$

$$C' = \frac{C}{L_a} \quad (6.4)$$

C and C' is related to λ. In this study, $\lambda = 532nm$. C can be estimated by equation 6.3-6.4, refers to [58]. Then C is equal to 4.96, when L_a=2nm, C' is equal to 0.62.

The results of L_a are shown in Fig 6.3:

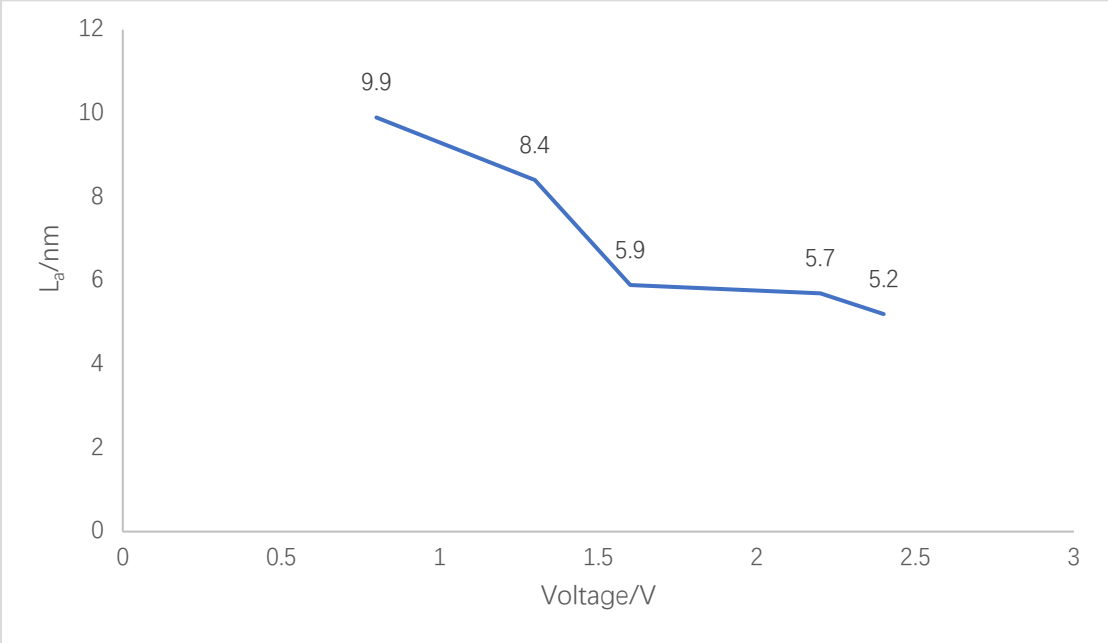

Fig 6.3 In-plane correlation length of CDCs as a function of voltage.

The graphitic crystallite size is decrease when voltage increase.

Table 6.1 shows the data discussed in this chapter.

Table 6.1 Voltage, I_D/I_G, Theoretical thickness and L_a

Voltage/V	I_D/I_G	Theoretical thickness/μm	L_a/nm
2.4	0.96	1.14	5.2
2.2	0.87	1.03	5.7
1.6	0.84	0.83	5.9
1.3	0.59	0.52	8.4
0.8	0.50	0.31	9.9

The results show that CDC formed even in relatively low voltage (less than one volt). The high mobility of lithium reaction product is one possible reason. The reaction product dissolve into either the nickel crucible or the graphite, which might also cause the phenomenon shown in Fig 5.14-5.15.

Conclusion

1. CDC can be produced by electrolysis in LiCl-KCl eutectic on carburized Ti-6Al-4V alloy substrate. This process can be done at 400℃ in 1 minute. The temperature and time required for CDC synthesis are much lower than previous studies using other synthesis methods. The results show that higher voltage in experiment, higher degree of electrolysis reaction took place.
2. CDCs produced in this study are characterized by Raman spectroscopy. By analyzing the Raman spectra, the degree of disorder in the CDC can be evaluated. The degree of disorder of CDC increase, as the voltage increase. The graphitic crystallite sizes in experiments are estimated from I_D/I_G. The graphitic crystallite size decreases when voltage increases.
3. The results show that CDC formed even in relatively low voltage (less than one volt). The high mobility of lithium reaction product is most possible reason, it dissolves into either the nickel crucible or the graphite, which might also be an explanation of the corrosion of Ni crucible and white crystals on the surface of graphite tube after experiments.

Reference

[1] Tallo, Indrek, et al. "Nanostructured carbide-derived carbon synthesized by chlorination of tungsten carbide." Carbon 49.13 (2011): 4427-4433.

[2] González-García, P., et al. "The production of carbon particles of different shapes produced by the chlorination of Cr (C5H5) 2." Carbon 52 (2013): 90-99.

[3] Samonin vv, Gk Ivakhnyuk, and Nf Fedorov. "MECHANISM OF INTERACTION OF CALCIUM CARBIDE WITH ALKALI-METAL CHLORIDES." JOURNAL OF APPLIED CHEMISTRY OF THE USSR 59.10 (1986): 2079-2083.

[4] Gogotsi, Yu G., and M. Yoshimura. "Formation of carbon films on carbides under hydrothermal conditions." Nature 367.6464 (1994): 628.

[5] Iijima, Sumio. "Graphitization of silicon carbide due to electron beam irradiation." Journal of Solid State Chemistry 42.1 (1982): 101-105.

[6] Wang, Shuyuan, and Guangjie Shao. "Silicon Carbide-Derived Carbon Prepared by Fused Salt Electrolysis and Electrochemical Performance." Journal of Nanomaterials 2016 (2016): 16.

[7] Yongjian Zhang. "The Deposition of Alkali Metal in the Process of $MgCl_2$ Elctrolysis" Doctoral dissertation.

[8] Zhongyu Yang. "QingJinShuYeJinXue." Beijing: Metallurgical Industry Press (1991).

[9] Kinoshita, Kim. "Carbon: electrochemical and physicochemical properties." (1988).

[10] Kroto, H. W. "The stability of the fullerenes Cn, with n= 24, 28, 32, 36, 50, 60 and 70." Nature 329.6139 (1987): 529.

[11] Iijima, S. "Helical microtubules of graphitic carbon Nature 354: 56–58." Find this article online (1991).

[12] Presser, Volker, Min Heon, and Yury Gogotsi. "Carbide‐derived carbons‐from porous networks to nanotubes and graphene." Advanced Functional Materials 21.5 (2011): 810-833.

[13] Kyotani, T., J. Chmiola, and Y. Gogotsi. "Carbon materials for electrochemical energy storage systems." (2010).

[14] Yeon, Sun-Hwa, et al. "Carbide-derived-carbons with hierarchical porosity from a preceramic polymer." Carbon 48.1 (2010): 201-210.

[15] Rose, Marcus, et al. "High surface area carbide-derived carbon fibers produced by electrospinning of polycarbosilane precursors." Carbon 48.2 (2010): 403-407.

[16] Gogotsi, Yury, et al. "Nanoporous carbide-derived carbon with tunable pore size." Nature materials 2.9 (2003): 591.

[17] Dash, Ranjan, et al. "Titanium carbide derived nanoporous carbon for energy-related applications." Carbon 44.12 (2006): 2489-2497.

[18] Chmiola, John, et al. "Monolithic carbide-derived carbon films for micro-supercapacitors." Science 328.5977 (2010): 480-483.

[19] Hutchins, Otis. "Method for the production of silicon tetrachlorid." U.S. Patent No. 1,271,713. 9 Jul. 1918.

[20] Mohun, W. A. "A novel amorphous carbon". In 4th Biennial Conference on Carbon(1959) : 443-53.

[21] Fedorov, N. F., G. K. Ivahnyuk, and V. V. Tetenov. "Carbon adsorbents based on silicon carbide." Zhurnal Prikladnoi Khimii(Leningrad) 54 (1981): 1464-8.

[22] Kormann, Martina, Helmut Gerhard, and Nadejda Popovska. "Comparative study of carbide-derived carbons obtained from biomorphic TiC and SiC structures." Carbon 47.1 (2009): 242-250.

[23] Kormann, Martina, et al. "Processing of carbide-derived carbon (CDC) using biomorphic porous titanium carbide ceramics." Journal of the European Ceramic Society 28.6 (2008): 1297-1303.

[24] Chun, Yoon-Soo, and Dae-Soon Lim. "Carbide derived carbon: from growth to tribological application." Journal of the Ceramic Society of Japan 122.1428 (2014): 577-585.

[25] Dash, R. K., A. Nikitin, and Yu Gogotsi. "Microporous carbon derived from boron carbide." Microporous and Mesoporous Materials 72.1-3 (2004): 203-208.

[26] Dash, R. K., G. Yushin, and Y. Gogotsi. "Synthesis, structure and porosity analysis of microporous and mesoporous carbon derived from zirconium carbide." Microporous and Mesoporous Materials 86.1-3 (2005): 50-57.

[27] Jänes, Alar, Thomas Thomberg, and Enn Lust. "Synthesis and characterisation of nanoporous carbide-derived carbon by chlorination of vanadium carbide." Carbon 45.14 (2007): 2717-2722.

[28] Batisse, Nicolas, et al. "Fluorination of silicon carbide thin films using pure F2 gas or XeF2." Thin Solid Films 518.23 (2010): 6746-6751.

[29] Fedorov, N. F., G. K. Ivakhnyuk, and V. V. Samonin. "Mesoporous carbon adsorbents from calcium carbide." JOURNAL OF APPLIED CHEMISTRY OF THE USSR 54.11 (1981): 2253-2255.

[30] Osetzky, D. "Macrocrystalline graphite from magnesium carbide." Carbon 12.5 (1974): 517-523.

[31] Fedorov, N. F., and V. V. Samonin. "Production, pore structure, adsorption properties, and fields of application of composite sorbents from calcium carbide." Russian journal of applied chemistry 71.5 (1998): 795-798.

[32] Fedorov, N. F., G. K. Ivakhnyuk, and V. V. Samonin. "Mesoporous carbon adsorbents from calcium carbide." JOURNAL OF APPLIED CHEMISTRY OF THE USSR 54.11 (1981): 2253-2255.

[33] Ferrari, Andrea Carlo, and John Robertson. "Raman spectroscopy of amorphous, nanostructured, diamond–like carbon, and nanodiamond." Philosophical Transactions of the Royal Society of London. Series A: Mathematical, Physical and Engineering Sciences 362.1824 (2004): 2477-2512.

[34] Gogotsi, Y. G., et al. "Formation of carbon coatings on SiC fibers by selective etching in halogens and supercritical water." The 22th Annual Conference on Composites, Advanced Ceramics, Materials and Structures: A. Am. Ceram. Soc., Westerville, OH, 1998.

[35] Kraft, T., K. G. Nickel, and Y. G. Gogotsi. "Hydrothermal degradation of chemical vapour deposited SiC fibres." Journal of materials science 33.17 (1998): 4357-4364.

[36] Kusunoki, Michiko, Masumi Rokkaku, and Toshiyuki Suzuki. "Epitaxial carbon nanotube film self-organized by sublimation decomposition of silicon carbide." Applied Physics Letters 71.18 (1997): 2620-2622.

[37] Euler F. Silicon “Carbide, a High Temperature Semiconductor.” Proceeding of the Conference on silicon carbide (1959).

[38] Iijima, Sumio. "Graphitization of silicon carbide due to electron beam irradiation." Journal of Solid-State Chemistry 42.1 (1982): 101-105.

[39] Foster, L. M., G. Long, and H. C. Stumpf. "Production of graphite single crystals by the thermal decomposition of aluminum carbide." American Mineralogist: Journal of Earth and Planetary Materials 43.3-4 (1958): 285-296.

[40] Gogotsi, Yury, et al. "Conversion of silicon carbide to crystalline diamond-structured carbon at ambient pressure." Nature 411.6835 (2001): 283.

[41] Presser, Volker, Min Heon, and Yury Gogotsi. "Carbide‐derived carbons‐from porous networks to nanotubes and graphene." Advanced Functional Materials 21.5 (2011): 810-833.

[42] S. Reich and C. Thomsen, “Raman spectroscopy of graphite,” Philosophical Transactions of the Royal Society A: Mathematical, Physical and Engineering Sciences, vol. 362, no. 1824, pp. 2271–2288, nov 2004.

[43] R. Beams, L. G. Cançado, and L. Novotny, “Raman characterization of defects and dopants in graphene,” Journal of Physics: Condensed Matter, vol. 27, no. 8, p. 083002, jan 2015.

[44] Evard, E. A., et al. "Kinetics of sorption and release of hydrogen by nanoporous carbon." Materials Science 36.4 (2000): 499-505.

[45] Schlapbach, Louis, and Andreas Züttel. "Hydrogen-storage materials for mobile applications." Materials for sustainable energy: a collection of peer-reviewed research and review articles from nature publishing group. 2011. 265-270.

[46] Gautier, S., et al. "Influence of the pyrolysis conditions on the nature of lithium inserted in hard carbons." The Journal of Physical Chemistry A 105.24 (2001): 5794-5800.

[47] Dash, Ranjan, et al. "Titanium carbide derived nanoporous carbon for energy-related applications." Carbon 44.12 (2006): 2489-2497.

[48] Kim, Hyun Seok, et al. "Molybdenum carbide-derived carbon for hydrogen storage." Microporous and Mesoporous Materials 120.3 (2009): 267-271.

[49] Yeon, Sun-Hwa, et al. "Enhanced methane storage of chemically and physically activated carbide-derived carbon." Journal of Power Sources 191.2 (2009): 560-567.

[50] Hoffman, Elizabeth N., et al. "Carbide-derived carbon membrane." Materials Chemistry and Physics 112.2 (2008): 587-591.

[51] Sridharan, Kumar, et al. Thermal properties of LiCl-KCl molten salt for nuclear waste separation. No. DOE/NEUP-09-780. Univ. of Wisconsin, Madison, WI (United States); Idaho National Laboratory (United States), 2012.

[52] Oberg, E., Jones, F., and Ryffel, H.(1989) Machinery's Handbook 23rd Edition. New York: Industrial Press Inc.

[53] Christiansen, Thomas L., and Marcel AJ Somers. "Stress and composition of carbon stabilized expanded austenite on stainless steel." Metallurgical and Materials Transactions A 40.8 (2009): 1791.

[54] Saleh, A. F., J. H. Abboud, and K. Y. Benyounis. "Surface carburizing of Ti–6Al–4V alloy by laser melting." Optics and Lasers in Engineering 48.3 (2010): 257-267.

[55] Zhao, Ziyuan, et al. "New strategy to grow TiC coatings on titanium alloy: Contact solid carburization by cast iron." Journal of Alloys and Compounds 745 (2018): 637-643.

[56] Lei, Zhu, et al. "State of Art for Study and Application of Supercapacitor [J]." Chinese Journal of Rare Metals 3 (2003).

[57] Nijkamp, M.G., et al. "Hydrogen storage using physisorption–materials demands." Applied Physics A 72.5 (2001): 619-623.

[58] McNallan, Michael, Mariusz Mika, and Kai-yuan Cheng. "Synthesis of carbide derived carbon (CDC) by electrolysis of molten chloride salts." Meeting Abstracts. No. 11. The Electrochemical Society, 2016.

[59] Various, Originlab Corp., Origin 2019b student version.

[60] Ferrari AC, Robertson J.et al. "Interpretation of Raman spectra of disordered and amorphous carbon. " Phys Rev B: Condens Mat Mater Phys 2000;61(20):14095–107.

[61] Jiang Xu. "Mechanism of Formation and Supercapacitive Performance of Carbide-Derived Carbon". Diss. Qinghuangdao: Yanshan University, 2015.

[62] Yani Sun. "Synthesis of Carbide Derived Carbon by Electrolysis in Molten Chlorides in Open Air". Chicago: University of Illinois, 2019.

[63] M. W. Chase, “NIST-JANAF thermochemical tables”, American institute of physics, 1998.

VITA

NAME:	Leqing Yang
EDUCATION:	B.A., Welding Technology and Engineering, Nanchang Hangkong University, Jiangxi, 2012
	M.S., Materials Engineering, University of Illinois at Chicago, Illinois, 2016